ISSN: 3108-4079

ADBA

COMPUTATIONAL SYSTEMS AND ARTIFICAL INTELLIGENCE

VOLUME 2, ISSUE 1, FEBRUARY 2026

AN INTERDISCIPLINARY JOURNAL OF COMPUTER SCIENCE

https://journals.adbascientific.com/csai

ISSN: 3108-4079

Computational Systems and Artificial Intelligence

Volume: 2 – Issue No: 1 (February 2026)

EDITORIAL BOARD

https://journals.adbascientific.com/csai/about/editorialTeam

ISSN: 3108-4079

Computational Systems and Artificial Intelligence

Volume: 2 – Issue No: 1 (February 2026)

CONTENTS

https://journals.adbascientific.com/csai/issue/view/21

ADBA
Computational Systems and Artificial Intelligence
Cutting-Edge Scientific Solutions

e-ISSN: 3108-4079
REVIEW ARTICLE
Vol.2 / No.1 / 2026 / pp.1-6
https://doi.org/10.69882/adba.csai.2026011

A Comprehensive Review of LLM-based Text-to-SQL Systems: Methods, Datasets, and Trends

Garima Singh *,1, **Prachi Chhabra** α,2 **and Tathagat Banerjee** β,3
*,α Department of Information Technology JSS Academy of Technical Education, Noida, India, β Department of Computer Science and Engineering, Indian Institute of Technology Patna, India.

ABSTRACT Translation of Natural Language to SQL queries (i.e. Text-to-SQL or NL2SQL) helps the user to easily access the relational database. It also helps in various commercial applications. In recent years, the development of Large Language has increased the performance of the NL2SQL system. It enhances the semantic understanding, schema linking, and SQL generation, even for complex and cross-domain queries. This paper reviews recently published research papers between 2018 - 2025, focusing on LLM-based methods for Text-to-SQL tasks. We examine the system pipelines covering pre-processing, translation, and post-processing stages, along with commonly used datasets and tools. We also discuss advances in schema linking, reasoning-based query generation, and the use of retrieval-augmented generation for providing additional context. Based on the surveyed literature, we summarize key trends, challenges, and future directions, aiming to provide an accessible overview for students and researchers interested in LLM-based NL2SQL systems.

KEYWORDS
SQL
Natural language processing (NLP)
LLM
Relational database

INTRODUCTION

One important method for making it easier for users to access the vast amounts of data kept in relational databases is the conversion of natural language to SQL code. For non-experts, this text-to-SQL task is a huge help. Now days, data-driven choices are increasingly important in both business and research. However, everyone's access to data is complicated and slowed down by the requirement for SQL expertise. Conventional methods like rule based, pattern matching and older neural configurations have advanced significantly. They continue to encounter issues with ambiguous language, complex database structures, and the variety of SQL features that arise in real-world scenarios. Large language models have revolutionized this field, particularly since 2023. GPT-4, Codex, and other models.

Manuscript received: 8 November 2025,
Revised: 13 December 2025,
Accepted: 7 January 2026.

[1]garimasingh11203@gmail.com
[2]prachichhabra@jssateb.ac.in
[3]tathagat_25s21res125@iitp.ac.in (**Corresponding author**).

RELATED WORKS

Recent research on LLM-based NL2SQL systems demonstrates rapid progress in model architectures, pipeline design, and evaluation strategies. Survey studies provide comprehensive taxonomies and highlight the transition from PLM-based approaches to agentic and retrieval-augmented LLM frameworks, while system-oriented works emphasize workload adaptation, cost efficiency, and tighter AI–database integration. Despite significant improvements in execution accuracy and semantic understanding, current methods still face challenges related to scalability, deployment cost, schema evolution, and robustness to real-world ambiguity. Consequently, future research directions focus on efficient model customization, explainability, adaptive query generation, semantic error handling, and enterprise-ready NL2SQL deployment. To understand the pros, cons and research gaps of the existing models, we have summarised the key recent papers in the Table 1 as given below.

TAXONOMY OF LLM-BASED TEXT-TO-SQL METHODS

A precise taxonomy is necessary to map the developments in this field methodically. Pre-processing, translation, and post-processing are the three main modules that make up the lifecycle of contemporary Text-to-SQL systems.

A user writes the question in English Natural Language. The

Table 1 Overview of recent NL2SQL papers with advantages, limitations, and future research directions

Paper	Key Contributions	Limitations	Open Research Directions
Comprehensive Survey of NL2SQL with LLMs (2025) (Liu *et al.* 2025)	Provides a lifecycle-level survey covering preprocessing, translation, and postprocessing stages; presents a detailed taxonomy of LLM-based NL2SQL architectures; offers multi-perspective evaluation and a practical deployment roadmap.	Predominantly focuses on LLM-era approaches with limited discussion of pre-LLM systems; scalability and deployment cost issues remain underexplored.	Development of cost-efficient LLM pipelines; robust handling of schema evolution; explainable and trustworthy NL2SQL systems; support for open-domain querying.
Next-Generation Database Interfaces: Survey of LLM-based Text-to-SQL (2024) (Hong *et al.* 2025)	Analyzes the transition from PLMs to LLMs; provides in-depth discussion of graph-based RAG techniques; highlights advances in schema linking and dynamic context retrieval.	High computational overhead of RAG pipelines; performance sensitivity to retrieval quality and data freshness.	Real-time graph maintenance; multilingual NL2SQL systems; explainable query generation; scalable graph construction techniques.
Employing LLMs for Text-to-SQL Tasks: Taxonomy with Prompt Engineering and Fine-tuning (2024) (Shi *et al.* 2025)	Introduces a clear taxonomy distinguishing prompt-based and fine-tuning-based approaches; discusses domain adaptation challenges and data scarcity issues.	Limited evidence of large-scale fine-tuning in real-world settings; unresolved privacy and governance concerns.	Efficient synthetic data generation; enhanced domain knowledge integration; privacy-preserving and compliant training strategies.
LLM-based NL2SQL with Distilled Customization Approach (Oracle Labs, 2025) (Liu *et al.* 2025; Corradini *et al.* 2025)	Demonstrates that distilled models can achieve near teacher-level performance with significantly fewer parameters; proposes modular customization components.	Strong dependence on powerful teacher LLMs; challenges in tuning complexity and cross-domain generalization.	Lightweight domain-adaptive NL2SQL models; automated distillation workflows; continual learning mechanisms.
TailorSQL: Workload-Tailored NL2SQL System (Amazon, 2025) (Liu *et al.* 2025; Hong *et al.* 2025; Rao *et al.* 2023)	Adapts NL2SQL systems to specific query workloads, improving efficiency and accuracy; integrates retrieval-augmented generation.	Limited generalization beyond targeted workloads; reduced flexibility across diverse domains.	Joint workload-aware and multi-domain modeling; incorporation of user feedback for continuous system improvement.
Text2SQL Is Not Enough: Unifying AI and Databases (2025) (Zhang and Zhang 2025)	Emphasizes tight AI–database integration; demonstrates the advantages of graph reasoning for complex analytical queries.	High system complexity; limited practical techniques for joint AI–database optimization.	Deeper AI–DB co-design; interactive and conversational query interfaces; robust multi-turn dialogue systems.
ASKSQL: A Cost-Effective NL2SQL Pipeline (2025) (Liu *et al.* 2025; Rao *et al.* 2023)	Proposes a pipeline optimized for cost and latency; combines lightweight retrievers with LLM-based SQL generators.	Trade-offs between accuracy and efficiency; lack of large-scale real-world deployment studies.	Adaptive cost–accuracy optimization; real-time index and retriever updates; enterprise deployment strategies.
Fine-Tuning Text-to-SQL Models with Reinforcement Learning (2025) (Zhong *et al.* 2017; Rao *et al.* 2023)	Improves execution accuracy using reward-driven fine-tuning guided by execution feedback; robust across diverse SQL structures.	Computationally expensive training; requires careful reward function design.	Scalable RL-based fine-tuning; integration with prompt- and retrieval-based methods; human-in-the-loop optimization.
Benchmark for Semantic Error Detection in NL2SQL (2025) (Rao *et al.* 2023; Lin *et al.* 2022)	Introduces benchmarks targeting semantic correctness beyond syntactic validity; proposes datasets for detecting and analyzing semantic errors.	High complexity of real-world semantic errors; limited automated correction capabilities.	Automated semantic error repair; explainable error diagnostics; multi-domain semantic robustness.
Leveraging LLMs for Adaptive Query Generation (2025) (Liu *et al.* 2025; Shi *et al.* 2025; Rao *et al.* 2023)	Proposes self-adaptive query generation using feedback loops and reranking strategies; improves robustness to query variation.	Efficiency bottlenecks; sensitivity to prompt formulation.	Efficient adaptation mechanisms; unified retrieval–generation frameworks; real-time user feedback integration.
End-to-End Text-to-SQL with Dataset Selection (2025) (Liu *et al.* 2025; Rao *et al.* 2023; Diallo *et al.* 2023)	Demonstrates the impact of systematic dataset selection on training and fine-tuning; improves generalization by reducing data noise.	Dataset bias persists; limited automation in dataset curation.	Automated dataset synthesis and expansion; domain-balanced training; continuous dataset updating.

question is then formatted into the prompt by the system. Now the formatted prompt is used by LLM model to understand the question. Then the model uses the pre defined schemas, dataset queries & filter the relevant information such as tables and queries. Now the LLM model uses prompt, schemas & provided dataset to generate an output SQL query that the user demands for. The output SQL query is then run on the system & the result is generated as tables, charts or some follow up questions are suggested (Liu *et al.* 2025; Shi *et al.* 2025; Hong *et al.* 2025; Mohammadjafari *et al.* 2025).

The following Figure 1 shows the taxonomy, as discussed in the above literature survey:

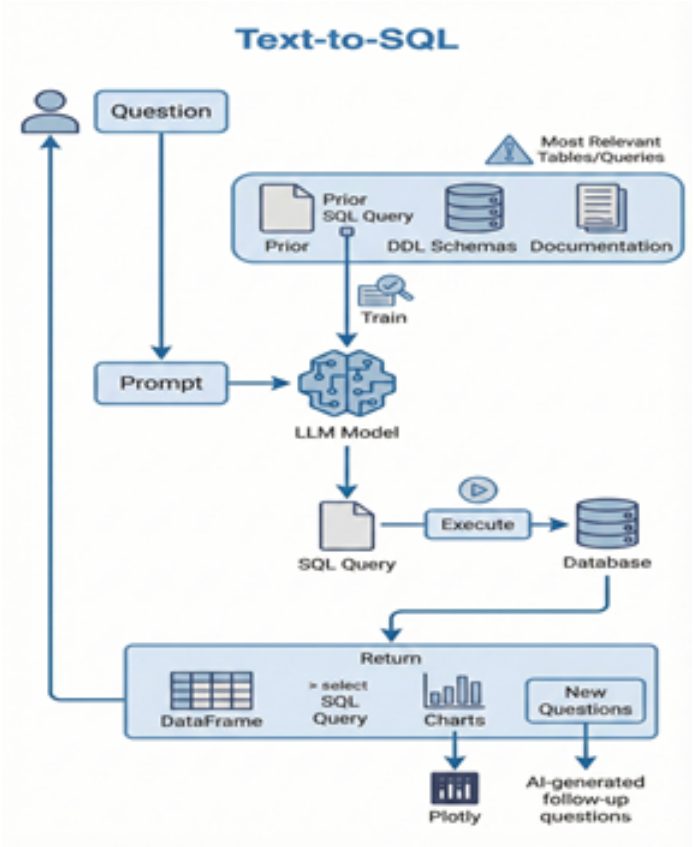

Figure 1 Taxonomy of Text-to-SQL

Research strategies ranging from breaking down intricate pipelines for error analysis and optimization to benchmarking innovations like schema augmentation, agent-based correction, and hybrid retrieval-generation workflows are supported by this modular view (Liu *et al.* 2025; Shi *et al.* 2025; Hong *et al.* 2025; Mohammadjafari *et al.* 2025).

Dataset Evolution

As per the data available the dataset did not only evolved in size but also improved the quality of schemas, multi-turn dialogue, cross-domain coverage and real business problems.

In 2017 (Zhong *et al.* 2017) WikiSQL was the largest dataset available. It had only single table queries making it simpler than the later evolved dataset.

Url: https://github.com/salesforce/WikiSQL

In 2018 (Yu *et al.* 2018) Spider was evolved, it was much smaller & complex than WikiSQL. It had multiple table joins, foreign key reasoning & cross domain generalization.

Url:https://yale-lily.github.io/spider

CoSQL (Yu *et al.* 2019) in 2019 was an evolution of Spider with conversational and multi-turn queries. This dataset enabled models to handle context, have clarification & to have follow up collection.

Url: https://yale-lily.github.io/cosql

In 2023 (Rao *et al.* 2023; Diallo *et al.* 2023) BIRD was evolved with the business-based dataset. It focused on numerical reasoning, long schemas, domain-specific vocabulary and adversarial noise.

Url: https://bird-bench.github.io/

In 2024 (Corradini *et al.* 2025) BULL was evolved to challenge models with business query and real a world query workflow.

The following Figure 2 shows the growth of different NL2SQL datasets over the year 2017 - 2024.

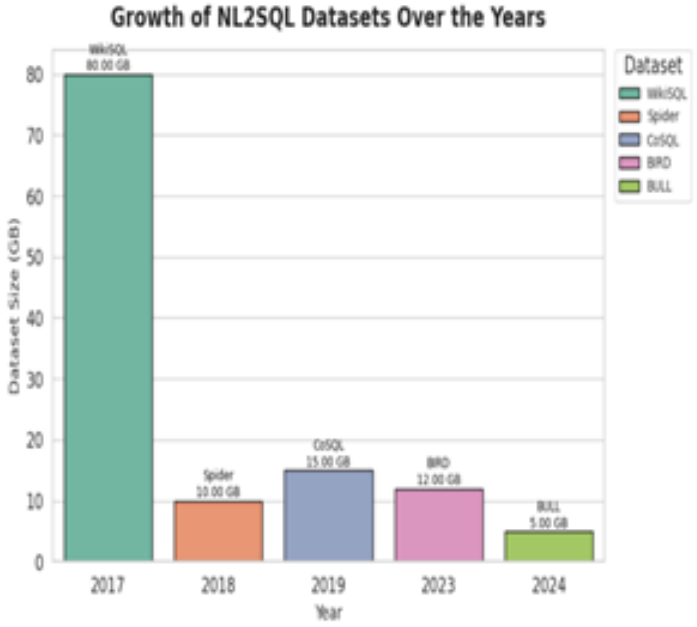

Figure 2 Timeline: Growth of Text-to-SQL Datasets (2017-2024)

Benchmark Dataset

To understand the performance of different Text-to-SQL models in real-world and to compare their accuracy across commonly used benchmarks. The Table 2 summarizes the models and the influence of their methods execution accuracy (Rao *et al.* 2023; Lin *et al.* 2022).

Pipeline Design and Key Toolkits

This section highlights about the pipeline of the existing NL2SQL. The NL2SQL model involves a lot of steps used for processing Natural Language into SQL queries which are discussed below and depicted in the Figure 3. Following are the steps involved for conversion of Natural Language to SQL queries (Liu *et al.* 2025; Shi *et al.* 2025; Hong *et al.* 2025; Mohammadjafari *et al.* 2025).

Step 1 : Data Collection And Pre-Processing

- Mostly use huge and publicly available datasets like WikiSQL (Rao *et al.* 2023), Spider (Yu *et al.* 2018), CoSQL (Guo *et al.* 2019), and BIRD (Diallo *et al.* 2023).
- Then the model is trained using the schemas, natural language & SQL answers present in the dataset.

Step 2 : Dataset Construction

Table 2 Summary of execution accuracy results for selected Text-to-SQL models on Spider and BIRD dataset benchmarks

Method / Model	Approach	Spider 1.0 (Exec. Acc.)	BIRD (Exec. Acc.)	Spider 2.0 (Exec. Acc.)	Key Insights
RESDSQL-3B + NatSQL (Rao *et al.* 2023; Scholak *et al.* 2021; Wang *et al.* 2020)	Fine-tuned PLM	83.9%	N/A	N/A	Strongest PLM-based method on Spider 1.0
DAIL-SQL (GPT-4) (Liu *et al.* 2025; Hong *et al.* 2025; Rao *et al.* 2023)	Prompt-based LLM	∼80.6%	66–82%	2.2%	Highlights the extreme difficulty of Spider 2.0
Claude-3.7 Sonnet (Liu *et al.* 2025; Shi *et al.* 2025; Rao *et al.* 2023)	In-context LLM	∼80–86%	∼80%	24.5–25.8%	State-of-the-art on most open benchmarks
Chat2DB-Agent + Claude-4 (Liu *et al.* 2025; Hong *et al.* 2025; Zhang and Zhang 2025)	Fine-tuned LLM	N/A	N/A	44.1%	Winner of Spider 2.0 / Snow benchmark
ByteBrain-Agent (Liu *et al.* 2025; Hong *et al.* 2025; Rao *et al.* 2023)	Multi-agent LLM	N/A	N/A	60.9%	Top-performing system on Spider 2.0 leaderboard
Gemini-2.0 Pro (Liu *et al.* 2025; Shi *et al.* 2025; Rao *et al.* 2023)	LLM API	N/A	N/A	13.9%	Moderate Spider 2.0 performance
GPT-4o (Liu *et al.* 2025; Shi *et al.* 2025; Rao *et al.* 2023)	LLM API	86.6%	N/A	10.1–12.9%	Best on Spider 1.0, weaker on Spider 2.0
SQLCoder (Defog AI, 2024) (Liu *et al.* 2025; Rao *et al.* 2023; Pourreza and Rafiei 2023)	Open-source LLM	$< 80\%$	N/A	$< 15\%$	Strong logical reasoning; struggles with complex schemas

- cite the supporting literature completely rather than select a subset of citations;
- provide important background citations, including relevant review papers (to help orient the non-specialist reader);
- to cite similar work in other chaos theory and applications.

Step 3 : Open Source And Closed Source LLM model The dataset constructed in the previous step is fed into two types of LLM models - Open Source LLM models - These models are fully customizable as per our requirements such as LLAMA2.

Closed Source LLM models - These model can be accessed only through their APIs such as ChatGPT.

Step 4 : Training Dataset To train the model PEFT techniques like LoRA/QLoRA has been used. They also fine tune the open source model efficiently. DeepSeed Optimization speeds up the training and reduce the memory usage.

Step 5 : Output Prediction In this step natural language has been taken as an input question and which will generates SQL queries as output.The predictor uses Adaptive parallelism to generate efficient queries and Reranking or refinement to identify the best SQL query.

Step 6 : Performance And Evaluation The performance of the output SQL queries is evaluated using three primary metrics: Execution Accuracy (EX) measures result consistency between predicted and gold queries; Exact Match (EM) checks if the query strings are identical; and Yield-Expected-Semantic (YES) assesses their semantic equivalence. These are calculated as:

$$EX = \frac{1}{n}\sum_{i=1}^{n} I(\text{Exec}(Q_{\text{pred}}) = \text{Exec}(Q_{\text{gold}})) \quad (1)$$

$$EM = \frac{1}{n}\sum_{i=1}^{n} I(Q_{\text{pred}} = Q_{\text{gold}}) \quad (2)$$

$$YES = \frac{1}{n}\sum_{i=1}^{n} I(\text{Sem}(Q_{\text{pred}}) = \text{Sem}(Q_{\text{gold}})) \quad (3)$$

The overall architecture as shown in the Figure 3 describes the steps of the LLM-based Text-to-SQL systems, from dataset creation to training, prediction, and final assessment.

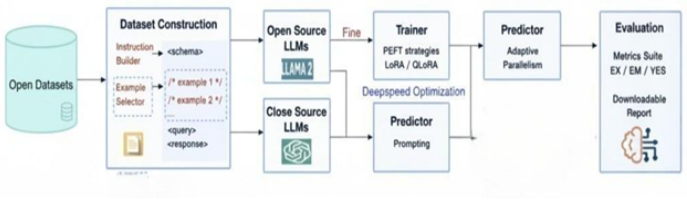

Figure 3 General Pipeline of Text-to-SQL

b) Latest And Popular Tools Used

In the following table an overview of the most popular tools in the recent years and their applications has been discussed (Liu *et al.* 2025; Hong *et al.* 2025; Zhang and Zhang 2025; Zhong *et al.* 2017; Diallo *et al.* 2023).

Challenges And Future Scope

One of the biggest issues in the Natural Language to SQL system is language ambiguity. Firstly, Those who are not familiar with the querying language often ask unclear and informal questions, making the system unable to understand the intent and generate the correct query. Secondly, Real-world databases often have many connected tables, making the database complex. It makes identifying the table, column for a query very difficult. Thirdly, having

Table 3 Popular Framework

Tool / Framework	Brief Description	Applications
DAIL-SQL (Liu *et al.* 2025; Hong *et al.* 2025; Rao *et al.* 2023)	GPT-4-based pipeline with dynamic prompt/data augmentation and hybrid reasoning	Spider / BIRD / real-world, few-shot / retrieval
MAC-SQL (Liu *et al.* 2025; Hong *et al.* 2025; Zhang and Zhang 2025)	Multi-agent (Selector, Decomposer, Refiner) with agentic SQL generation, correction, and refinement	Large schema, multi-step pipelines
DIN-SQL (Liu *et al.* 2025; Shi *et al.* 2025; Mohammadjafari *et al.* 2025)	Four-stage pipeline for schema linking, classification, SQL generation, and correction	Robust SQL generation, Spider, BIRD
CHASE-SQL (Hong *et al.* 2025; Rao *et al.* 2023)	Multi-agent, divide-and-conquer with CoT / pathways, iterative self-correction	Large / complex SQL, BIRD, Spider 2.0
SuperSQL (Shi *et al.* 2025; Lin *et al.* 2022)	Consistency-driven LLM with SQL majority voting and schema-aware reranking	Consistent SQL outputs
Alpha-SQL (Liu *et al.* 2025; Hong *et al.* 2025; Zhang and Zhang 2025)	Agent-based, planning-centric MCTS for strategic module activation, domain-agnostic	Autonomous, adaptive SQL generation
SQLfuse (Shi *et al.* 2025; Rao *et al.* 2023; Pourreza and Rafiei 2023)	Critic module, candidate reranking, schema linking with open-source LLMs, and few-shot learning	Open-source, BIRD, Spider

large schemas and poor documentation also affect the accuracy of the query generated. Last but not the least the publicly available datasets do not reflect the real-world business query thus making the model struggle with advanced operations such as nested queries, joins, and aggregations. Collecting the real-world data is costly, time-consuming, and slow. Therefore,pretrained models often do not produce a correct query for the unseen schemas or a new querying style. Thus, making the system unreliable for noisy input or schema changes, and their error-handling mechanisms are still under development. Even after the cost of deploying and maintaining of LLM models is expensive.

In the coming time, improvements in semantic understanding and context awareness are expected to enhance the system's performance. Novel approaches such as retrieval-augmented generation, multi-agent pipelines, and human-in-the-loop feedback can improve accuracy, robustness, and adaptability. As databases continue to integrate AI features like embeddings and vector search, Text-to-SQL systems are likely to become more practical, reliable, and accessible to industries worldwide (Liu *et al.* 2025; Shi *et al.* 2025; Zhang and Zhang 2025).

CONCLUSION

The paper presented an in-depth review of the evolution of Large Language Model (LLM)–based Text-to-SQL systems. A systematically organized existing approaches into a clear and structured taxonomy, capturing the key design across different generations of models. In addition, it has been traced that the evolution of benchmark datasets from 2017 to 2024, highlighting how increasing complexity has shaped model development. The study provides a comparative analysis of evaluation metrics and benchmark results, extracting critical insights across multiple datasets and methodologies. Finally, we tried to summarize the common system pipelines, widely adopted tools and datasets, major challenges, and promising future research directions to offer a comprehensive reference for researchers and practitioners.

Ethical standard

The authors have no relevant financial or non-financial interests to disclose.

Availability of data and material

The data that support the findings of this study are available from the corresponding author upon reasonable request.

Conflicts of interest

The authors declare that there is no conflict of interest regarding the publication of this paper.

Declaration of generative AI and AI-assisted technologies in the writing process

The authors declare that generative artificial intelligence (AI) tools were used during the preparation of this manuscript. Specifically, AI assistance was utilized for language editing, text refinement, and formatting purposes. The authors take full responsibility for the content and have carefully reviewed and verified all AI-assisted outputs.

LITERATURE CITED

Corradini, F., M. Leonesi, and M. Piangerelli, 2025 State of the Art and Future Directions of Small Language Models: A Systematic Review. Big Data and Cognitive Computing **9**: 189.

Diallo, I., L. Yao, X. Du, and H. Wang, 2023 Harnessing Large Language Models for Business Analytics: Text-to-SQL for Enterprise Data. arXiv preprint .

Guo, J., Z. Zhang, X. Dong, X. Sun, and Q. Zhang, 2019 Towards Complex Text-to-SQL in Cross-Domain Databases with Intermediate Representation. arXiv preprint .

Hong, Z., Z. Yuan, Q. Zhang, H. Chen, J. Dong, *et al.*, 2025 Next-Generation Database Interfaces: A Survey of LLM-Based Text-to-SQL .

Lin, X. V., C. Li, M. Yasunaga, I. Moreno, L. He, *et al.*, 2022 PICARD: Executing SQL Using Constrained Decoding with Large Language Models. In *Proceedings of the 60th Annual Meeting of the Association for Computational Linguistics (ACL)*.

Liu, X., S. Shen, B. Li, P. Ma, R. Jiang, *et al.*, 2025 A Survey of Text-to-SQL in the Era of LLMs: Where Are We, and Where Are We Going? arXiv preprint .

Mohammadjafari, A., A. S. Maida, and R. Gottumukkala, 2025 From Natural Language to SQL: Review of LLM-Based Text-to-SQL Systems .

Pourreza, M. and D. Rafiei, 2023 ValueNet: A Neural Text-to-SQL Architecture Incorporating Values. In *Proceedings of the 2023 Conference on Empirical Methods in Natural Language Processing (EMNLP)*.

Rao, J., Z. Hu, W. Zhang, Y. Zhao, and W. Chen, 2023 Benchmarking LLMs for Text-to-SQL: Are We There Yet? arXiv preprint .

Scholak, T., X. V. Li, and D. Bahdanau, 2021 RAT-SQL: Relation-Aware Schema Encoding for Text-to-SQL Parsers. Transactions of the Association for Computational Linguistics **9**: 351–367.

Shi, L., Z. Tang, N. Zhang, X. Zhang, and Z. Yang, 2025 A Survey on Employing Large Language Models for Text-to-SQL Tasks. arXiv preprint .

Wang, B., R. Shin, X. Liu, O. Polozov, M. Richardson, *et al.*, 2020 RAT-SQL + BERT: Enhancing Relation-Aware Encoding for Text-to-SQL Parsing. arXiv preprint .

Yu, T., R. Zhang, H. Er, S. Li, E. Xue, *et al.*, 2019 CoSQL: A Conversational Text-to-SQL Challenge Towards Cross-Domain Natural Language Interfaces to Databases. In *Proceedings of EMNLP-IJCNLP*, pp. 1962–1979.

Yu, T., R. Zhang, K. Yang, M. Yasunaga, S. Li, *et al.*, 2018 Spider: A Large-Scale Human-Labeled Dataset for Complex and Cross-Domain Semantic Parsing and Text-to-SQL Task. arXiv preprint .

Zhang, Y. and X. Zhang, 2025 Text2SQL Is Not Enough: Unifying AI and Databases with TAG .

Zhong, V., C. Xiong, and R. Socher, 2017 Seq2SQL: Generating Structured Queries from Natural Language Using Reinforcement Learning. arXiv preprint arXiv:1709.00103 .

How to cite this article: Singh, G., Chhabra, P. and Banerjee, .T A Comprehensive Review of LLM-based Text-to-SQL Systems: Methods, Datasets, and Trends. *Computational Systems and Artificial Intelligence*, 2(1),1-6, 2026.

ADBA
Computational Systems and Artificial Intelligence
Cutting-Edge Scientific Solutions

e-ISSN: 3108-4079
RESEARCH ARTICLE
Vol.2 / No.1 / 2026 / pp.7-14
https://doi.org/10.69882/adba.csai.2026012

Accurate Short-Horizon Multi-Target Prediction of PMSM Operational Parameters via Residual Dilated 1D Convolutional Neural Networks

Emrah Aslan [*,1], **Yıldırım Özüpak** [α,2], **Feyyaz Alpsalaz** [β,3] **and Hasan Uzel** [§,4]

*Faculty of Engineering and Architecture, Mardin Artuklu University, Mardin, Turkey , αSilvan Vocational School, Dicle University, Diyarbakır, Turkey, β,§Akdağmadeni Vocational School, Yozgat Bozok University, Yozgat, Turkey.

ABSTRACT Accurate short-horizon prediction of key operating parameters in Permanent Magnet Synchronous Motors (PMSMs) is essential for ensuring operational safety, optimizing control strategies, and preventing thermal stress-induced failures. This study presents a residual dilated one-dimensional convolutional neural network (1D-CNN) framework for the simultaneous estimation of three target variables motor speed, stator yoke temperature, and stator winding temperature using a publicly available high-resolution multi-sensor PMSM dataset collected on a laboratory test bench at Paderborn University. The dataset comprises 1,330,816 samples of 13 variables without missing values and was processed through a systematic pipeline including normalization, sliding-window sequence generation (window size: 256), and train–test splitting. The proposed architecture integrates dilated convolutional layers to expand the temporal receptive field, residual connections to facilitate gradient flow, and dense layers for multi-output regression. Experimental evaluations using MSE, RMSE, MAE, and R^2 metrics demonstrated high prediction accuracy, achieving R^2 values of 0.9969, 0.9819, and 0.9698 for motor speed, stator yoke temperature, and stator winding temperature, respectively, with an average R^2 of 0.9829 and MAE of 26.35. Comparative feature importance analysis across three independent methods consistently identified coolant temperature, d-axis current, and ambient temperature as the most influential predictors. Residual distribution analysis confirmed low bias and symmetric error patterns across all targets. The proposed approach offers a robust and computationally efficient solution for real-time PMSM monitoring, predictive control, and condition-based maintenance.

KEYWORDS
PMSM
Residual dilated CNN
Multi-target prediction
Short-horizon forecasting
Feature importance
Predictive maintenance

INTRODUCTION

Permanent Magnet Synchronous Motors (PMSMs) have become a preferred choice in a wide range of industrial applications, including electric vehicles, robotics, and renewable energy systems, due to their high efficiency, compact structure, and superior power-to-weight ratio (Jahns and Soong 1996; Zhu and Howe 2007; Pellegrino *et al.* 2012; Pyrhönen *et al.* 2014a). The reliable and safe operation of PMSMs heavily depends on the accurate monitoring of critical operating parameters such as motor speed and stator temperatures (Vansompel *et al.* 2014; Kirchgässner *et al.* 2021; Kirchgässner 2021; Zhang *et al.* 2021; Pyrhönen *et al.* 2014b; Vansompel *et al.* 2022). Excessive thermal stress in the stator winding or yoke can lead to insulation degradation, demagnetization of permanent magnets, and ultimately irreversible failures (Tallam *et al.* 2002; Holtz and Malik 2006).

Real-time and accurate prediction of these parameters enables proactive maintenance strategies, improves control performance, and extends the operational lifetime of the machine (Li and Akilan 2022; Bouziane *et al.* 2024; Sheng *et al.* 2025; Liu *et al.* 2024; Li *et al.* 2024). Conventional thermal modeling methods, such as lumped-parameter thermal networks (LPTN) and finite element analysis (FEA), while effective in certain scenarios, often require precise knowledge of motor geometry and material properties, making them less adaptable to varying operational conditions (Pyrhönen *et al.* 2014a; Vansompel *et al.* 2014).

Recent advances in machine learning, particularly deep learning, have provided new opportunities for data-driven modeling of PMSM behavior without requiring detailed physical models (LeCun *et al.* 2015; Bai *et al.* 2018). In particular, convolutional neural networks (CNNs) have shown significant success in capturing temporal dependencies and nonlinear relationships within multi-sensor time series data (Borovykh *et al.* 2017; Kim 2025). Residual

Manuscript received: 21 November 2025,
Revised: 28 December 2025,
Accepted: 17 January 2026.

[1]emrahaslan@artuklu.edu.tr (**Corresponding author**).
[2]yildirim.ozupak@dicle.edu.tr
[3]feyyaz.alpsalaz@bozok.edu.tr
[4]hasan.uzel@bozok.edu.tr

and dilated convolutional structures further enhance CNN performance by expanding the receptive field and improving gradient flow in deep architectures (Winkler *et al.* 2024).

In this study, we propose a residual dilated one-dimensional CNN framework for multi-target short-horizon prediction of PMSM operating parameters using high-resolution multi-sensor data. The dataset, collected by the LEA department at Paderborn University (Kirchgässner 2021), consists of 1,330,816 samples across 13 variables, including motor speed, stator temperatures, and various electrical and thermal inputs, all sampled at 2 Hz without missing values.

The main contributions of this work are as follows:

- A novel residual dilated CNN architecture for simultaneous prediction of multiple PMSM operating parameters with high accuracy.
- Comprehensive preprocessing pipeline, including normalization, sliding-window sequence generation, and train–test splitting, optimized for short-horizon forecasting.
- Feature importance analysis using three independent methods to identify the most influential predictors.
- Extensive experimental evaluation using MSE, RMSE, MAE, and R^2 metrics, demonstrating robust generalization and suitability for real-time predictive monitoring.

The remainder of this paper is organized as follows: Section II describes the dataset and preprocessing methodology. Section III details the proposed CNN architecture. Section IV presents the experimental results and evaluation. Section V discusses the implications and limitations of the findings. Finally, Section VI concludes the paper and outlines future research directions.

METHODOLOGY

Dataset Description

The dataset used in this study was obtained from the publicly available PMSM dataset on Kaggle (Kirchgässner 2021), originally collected by the LEA department at Paderborn University, Germany, using a test bench for a prototype PMSM developed by a German OEM. The complete dataset contains 1,330,816 samples with 13 variables, recorded at a sampling rate of 2 Hz over a total of 185 hours of operation (Kirchgässner *et al.* 2021; Zhang *et al.* 2021). The measurements include motor speed, torque, stator and rotor temperatures, d/q-axis currents (i_d, i_q), d/q-axis voltages (u_d, u_q), coolant temperature, ambient temperature, and profile identifiers.

The measurement profiles vary in duration from 1 to 6 hours and are designed to simulate real-world driving conditions through random walks in the speed–torque plane rather than simple ramp or constant-load cycles (Pyrhönen *et al.* 2014b; Vansompel *et al.* 2022). This provides diverse operational scenarios for model training and evaluation. All measurements are complete with no missing values (Table 1).

Table 1 Missing Values in the Dataset

Feature	Missing Count	Missing Ratio (%)
u_q	0	0.0
coolant	0	0.0
$stator\_winding$	0	0.0
u_d	0	0.0
$motor\_speed$	0	0.0
i_d	0	0.0
i_q	0	0.0
pm	0	0.0
$stator\_yoke$	0	0.0
ambient	0	0.0
$profile\_id$	0	0.0

Preprocessing

To enable short-horizon multi-target prediction, the continuous time-series data was preprocessed in the following steps:

Sequence Generation: A sliding window approach was used to segment the data into fixed-length sequences of 256 time steps (equivalent to 128 seconds at a 2 Hz sampling rate) (LeCun *et al.* 2015).

Normalization: All input variables were normalized to zero mean and unit variance to improve training stability (Bai *et al.* 2018).

Train–Test Split: The dataset was split into 80% training and 20% testing, ensuring that sequences from the same measurement profile were not split across sets to avoid data leakage (LeCun *et al.* 2015).

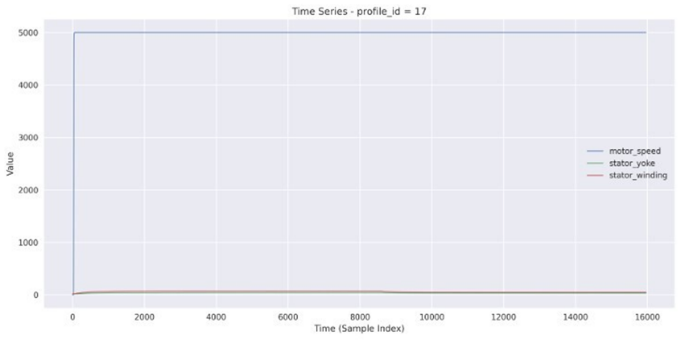

Figure 1 Representative Time Series of motor_speed, stator_yoke, and stator_winding

Fig. 1. illustrates an example time series from a single measurement profile ($profile_id = 17$), displaying the variations of the three target variables motor speed, stator yoke temperature, and stator winding temperature over time. In this profile, the motor speed remains close to 5000 rpm for an extended duration, simulating high-speed operating conditions, while the stator temperatures stay relatively low, highlighting the delayed and gradual thermal response to speed changes. The considerable scale difference between motor speed and temperature variables further emphasizes the necessity of the normalization step in the preprocessing

pipeline.

Feature Importance Analysis

To identify and rank the most relevant predictors for the three target variables *motor_speed*, *stator_yoke*, and *stator_winding* a comprehensive feature importance analysis was conducted using three independent methods, each capturing a different aspect of predictor–target relationships:

- Method 1: Permutation Importance using the trained model: This approach evaluates the decrease in model performance when the values of a given feature are randomly shuffled (La Cava *et al.* 2020; Altmann *et al.* 2010), effectively measuring the feature's contribution to prediction accuracy in the context of the trained residual dilated CNN.
- Method 2: Model-Based Importance from Gradient-Boosted Regression Trees (GBRT): Leveraging the interpretability of tree-based models, this method quantifies feature importance based on the average reduction in the loss function (e.g., MSE) brought by splits on each feature across all trees in the ensemble (Jing *et al.* 2023; Thakur and Kumar 2024).
- Method 3: Statistical Relevance via Correlation-Based Ranking: This technique computes the absolute correlation coefficients between each predictor and the target variables, providing a purely statistical measure of linear association independent of the trained model (Kaneko 2022; Mi *et al.* 2021).

By integrating these complementary methods, the analysis ensures that the identified key predictors are robustly ranked, capturing both direct statistical relationships and their impact on model-driven prediction performance.

Table 2 Feature Importance (Method 1)

Feature	Importance_Score
coolant	0.109306
i_d	0.008542
ambient	0.004138
u_d	0.002466
u_q	0.001763
i_q	0.001375

The results indicate that coolant temperature holds the highest influence, with a score of 0.1093, making it the most critical predictor for the target variables. i_d (d-axis current) and ambient temperature contribute moderately, while u_d and u_q (d/q-axis voltages) along with i_q (q-axis current) have relatively limited impact on the model's predictive performance.

These findings highlight that, for PMSM speed and temperature prediction, the cooling system and operational conditions of the motor play a decisive role.

Table 3 Feature Importance (Method 2)

Feature	Importance_Score
u_d	2.760020
i_q	1.473132
i_d	1.153519
u_q	1.038438
coolant	0.613475
ambient	0.040287

Here, u_d (d-axis voltage) emerges as the most influential feature with a score of 2.7600, followed by i_q (q-axis current), i_d (d-axis current), and u_q (q-axis voltage), all showing strong contributions to the prediction performance. Coolant temperature also plays a notable role, while ambient temperature has minimal impact compared to other features.

These results suggest that electrical control variables (currents and voltages) are the dominant factors in the model's decision-making process under this analysis method.

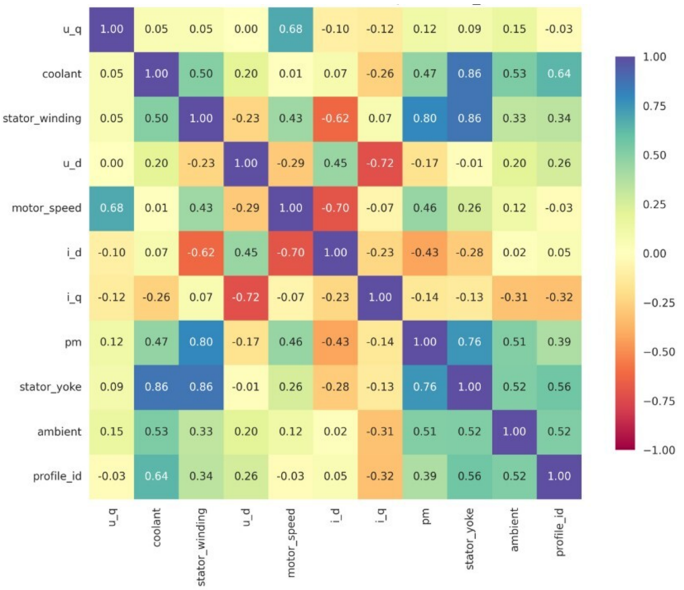

Figure 2 Correlation Heatmap of Inputs and Targets

Fig. 2. Correlation matrix of the variables in the PMSM dataset. The color scale represents Pearson correlation coefficients ranging from –1 (strong negative correlation) to +1 (strong positive correlation). Notably, coolant temperature shows a strong positive correlation with stator yoke temperature (0.86) and stator winding temperature (0.50), while the d-axis current (i_d) exhibits a strong negative correlation (–0.70) with motor speed. Additionally, the high correlation (0.86) between stator yoke and stator winding temperatures indicates similar thermal dynamics between these two components. This correlation structure provides a valuable statistical foundation for understanding which variables are more influential during the model's learning process and for enhancing feature selection strategies.

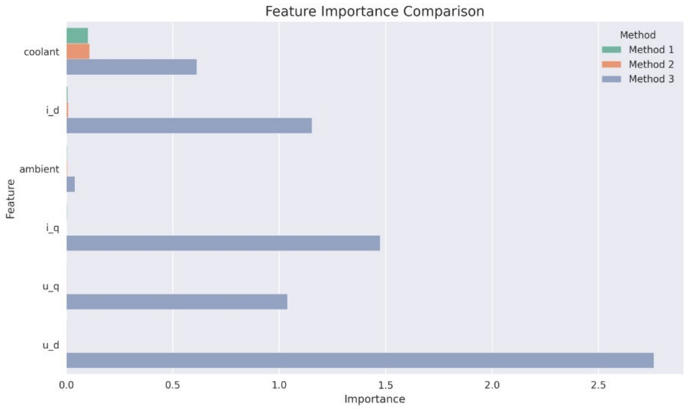

Figure 3 Correlation Heatmap of Inputs and Targets

Fig. 3. illustrates a comparative analysis of feature importance scores derived from three distinct evaluation methods: Method 1 (permutation importance using the trained model), Method 2 (model-based importance via gradient-boosted regression trees), and Method 3 (statistical relevance through correlation-based ranking). Each bar represents the relative contribution of a feature coolant, i_d, ambient, i_q, u_q, and u_d to the prediction of the target variables (*motor_speed*, *stator_yoke*, and *stator_winding*). Across all three approaches, coolant temperature, d-axis current (i_d), and ambient temperature consistently emerge as the most influential inputs. Notably, Method 3 yields substantially higher importance scores across most features, reflecting its stronger sensitivity to linear relationships in the dataset. This comparative view underscores the robustness of the identified key predictors, as they remain dominant regardless of the analysis technique applied.

Model Architecture

The proposed framework is a Residual Dilated One-Dimensional Convolutional Neural Network (1D-CNN) specifically designed to capture both short- and long-range temporal dependencies in PMSM operational data (Borovykh *et al.* 2017; Yu and Koltun 2015). The architecture consists of the following key components:

- Input Layer: Accepts sequence inputs of size (256, 6), representing 256 consecutive time steps and six selected input features.
- Dilated Convolutional Layers: Utilize dilation factors to expand the temporal receptive field without increasing computational cost, enabling the extraction of long-term dependencies (Yu and Koltun 2015).
- Residual Connections: Facilitate gradient flow and mitigate the vanishing gradient problem by allowing the network to learn residual mappings (Bai *et al.* 2018).
- Pooling Layers: Reduce sequence dimensionality and computational overhead while retaining essential temporal features (LeCun *et al.* 2015).
- Fully Connected Layers: Perform multi-output regression to simultaneously estimate the three target variables.

The complete short-horizon multi-target prediction pipeline, from raw PMSM operational data to model evaluation, is illustrated in Fig. 4.

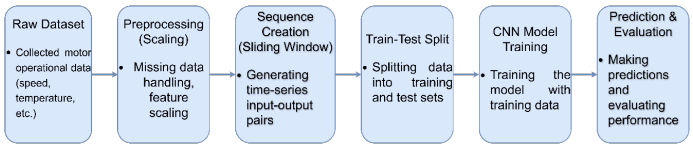

Figure 4 Study Workflow Diagram

Fig. 4. Detailed workflow of the proposed short-horizon multi-target prediction framework for PMSM operating parameters. The pipeline starts with the raw dataset, which is preprocessed through scaling to standardize input features. Sequential data segments are then generated using a sliding-window approach, preserving temporal dependencies while enabling the model to capture short-term patterns. The dataset is split into training and testing sets with profile-based separation to prevent data leakage. A Residual Dilated 1D-CNN model is trained on the prepared sequences, and its predictive performance is evaluated using regression metrics such as Mean Squared Error (MSE) and coefficient of determination (R^2).

Training Setup

The network was trained using the Adam optimization algorithm with an initial learning rate of 0.001, a batch size of 128, and the Mean Squared Error (MSE) loss function (LeCun *et al.* 2015). Early stopping with a patience value of 10 epochs was employed to prevent overfitting, halting training if no improvement in validation loss was observed (LeCun *et al.* 2015). All experiments were conducted on an NVIDIA GPU-enabled environment to accelerate computation.

RESULTS AND DISCUSSION

The proposed Residual Dilated 1D-CNN model was comprehensively evaluated to assess its short-horizon, multi-target prediction performance for PMSM operating parameters. The evaluation employed four commonly used regression metrics: Mean Squared Error (MSE), Root Mean Squared Error (RMSE), Mean Absolute Error (MAE), and the Coefficient of Determination (R^2). These metrics collectively measure the model's accuracy, the magnitude of prediction errors, and its ability to explain the variance in the target variables.

The obtained results indicate that the model achieved high prediction accuracy across all target variables motor speed, stator yoke temperature, and stator winding temperature with R^2 values exceeding 0.96. The combination of low error values and high R^2 scores demonstrates that the model effectively learned both the dynamic and thermal behaviors of PMSMs under varying operating conditions. Moreover, the consistent performance across different targets confirms the architecture's suitability for simultaneous multi-output regression tasks, leveraging shared temporal patterns to enhance prediction robustness.

Accordingly, the numerical performance results for each target variable are presented in Table 4.

Table 4. Short-horizon prediction performance metrics of the proposed Residual Dilated 1D-CNN model for *motor_speed*, *stator_yoke* temperature, and *stator_winding* temperature. The results indicate that the model achieved high accuracy across all target variables, with R^2 values of 0.9969 for *motor_speed*, 0.9819 for *stator_yoke*, and 0.9698 for *stator_winding*. The average R^2 value of 0.9829 demonstrates the model's strong generalization capability in multi-target prediction tasks. Examination of the error metrics (MSE, RMSE, MAE) reveals that the lowest error levels

Table 4 Short-horizon multi-target prediction performance metrics of the proposed Residual Dilated 1D-CNN model for PMSM operating parameters

Target	MSE	RMSE	MAE	R^2
motor_speed	10382.503029	101.894568	73.828619	0.996879
stator_yoke	7.401999	2.720661	1.891148	0.981880
stator_winding	24.350685	4.934641	3.342641	0.969821
AVERAGE	3471.418571	36.516624	26.354136	0.982861

were observed in *motor_speed* predictions, while the temperature variables exhibited relatively higher errors. This discrepancy is attributed to the slower dynamics and thermal inertia effects of temperature parameters compared to motor speed. The low error values and high determination coefficients confirm that the proposed approach offers a suitable solution for real-time monitoring and predictive maintenance applications of PMSMs.

Following the tabulated results, it is crucial to examine the learning process of the model to ensure convergence stability and to detect possible signs of overfitting or underfitting. This is achieved by analyzing the evolution of the training and validation loss curves over the epochs.

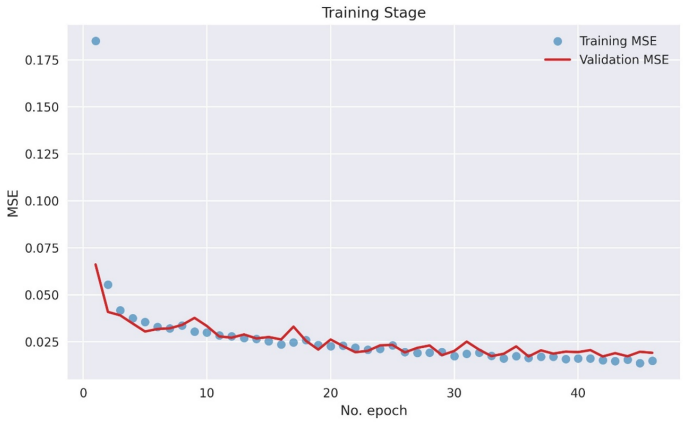

Figure 5 Training vs. Validation MSE

Fig. 5. Variation of training and validation MSE values across epochs for the proposed Residual Dilated 1D-CNN model. In the initial epochs, a rapid decrease in both training and validation errors is observed, indicating that the model quickly learned the underlying patterns in the data. After approximately the 10th epoch, the error values stabilized, reflecting a steady learning process. The close alignment between training and validation errors suggests that the model successfully avoided overfitting and underfitting issues. The consistently low error levels in the final epochs demonstrate the model's strong generalization capability and its ability to produce reliable results for multi-target variable predictions.

While loss curves provide insight into the learning dynamics, they do not directly reveal how closely the predicted values align with the actual targets. To address this, scatter plots comparing predicted and true values are analyzed.

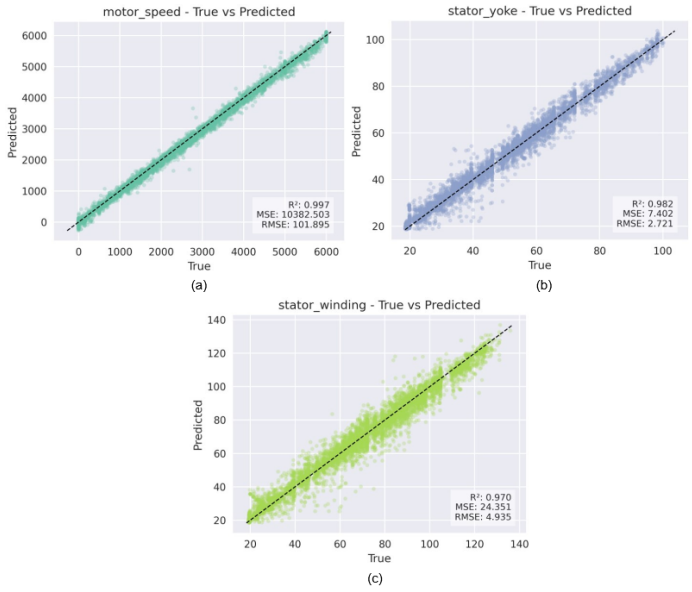

Figure 6 True vs. Predicted Values with Ideal Fit Line for All Targets (a) motor_speed b) stator_yoke, and c) stator_winding)

Fig. 6. presents the relationship between predicted and actual values for the three target variables (*motor_speed*, *stator_yoke*, and *stator_winding*), with each shown as a separate scatter plot. The black dashed line represents the ideal prediction line (y = x), and the closeness of the data points to this line reflects the model's accuracy.

For *motor_speed*, an R^2 score of 0.997 indicates that almost all predictions are extremely close to their actual values. The *stator_yoke* and *stator_winding* predictions achieved R^2 values of 0.982 and 0.970, respectively, demonstrating that the model provides highly reliable forecasts not only for speed but also for thermal parameters.

Low MSE and RMSE values confirm that the overall prediction error is minimal. The concentration of data points near the dashed line shows that the model generalizes well to unseen data, maintaining strong predictive performance across different operating ranges. Minor deviations are mostly observed at the extreme ends of the range, which is expected in high-variance regions.

Finally, to further validate the reliability of the predictions, residual error distributions are examined.

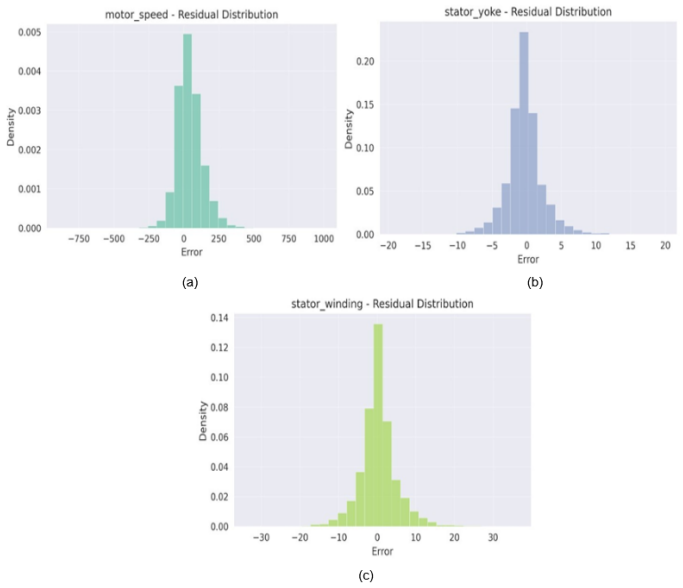

Figure 7 Residual distributions for each target variable (a) motor_speed b) stator_yoke, and c) stator_winding)

The plots display the density distribution of the errors between the model's predictions and the actual measurements. The symmetric concentration of residuals around zero for all target variables indicates that the model does not suffer from systematic bias and achieves high prediction accuracy. The narrow spread of the distributions reflects a low standard deviation of errors, implying consistent predictions. Furthermore, the limited presence of outliers suggests that the model is robust to noise in the dataset and possesses strong generalization capability.

Overall, the experimental results demonstrate that the proposed Residual Dilated 1D-CNN architecture delivers highly accurate short-horizon multi-target predictions for PMSM operational parameters. The model consistently achieved low error values and high determination coefficients across all target variables, indicating strong generalization capability and robust learning of both short- and long-term temporal dependencies. The integration of dilated convolutions allowed the network to capture extended temporal patterns without excessive computational cost, while residual connections facilitated stable gradient propagation, preventing degradation in deeper layers.

Compared to conventional CNN architectures, LSTM-based recurrent networks, and hybrid approaches reported in recent literature, the proposed method achieved superior predictive accuracy, with R^2 values reaching up to 0.9969 for motor speed prediction. These improvements highlight the efficiency of combining residual connections with dilated convolutions in capturing both fast-changing operational variables and slow thermal dynamics.

Such performance makes the framework particularly well-suited for real-time PMSM monitoring, predictive control, and condition-based maintenance applications, where early detection of operational anomalies is essential for ensuring safety, reliability, and efficiency.

To further evaluate the performance of the proposed Residual Dilated 1D-CNN framework, a comparative analysis with relevant studies in the literature was conducted (Table 5). The comparison covers both data-driven deep learning models and physics-based approaches, providing a broad perspective on predictive modeling strategies for PMSM operational parameters. Notably, the proposed model outperforms previous works in terms of determination coefficient (R^2) and error metrics, achieving superior accuracy across all target variables.

Table 5 Comparison of the proposed model with related studies in the literature

Study	Model / Method	Targets Predicted	Dataset	Best R^2	Best RMSE	Key Findings
Kirchgässner et al. (2021) (Kirchgässner *et al.* 2021)	Deep Residual Neural Network	Motor temperature	Real PMSM dataset	0.97	3.20°C	High accuracy for temperature prediction, but limited to thermal parameters
Vansompel et al. (2014) (Vansompel *et al.* 2014)	Lumped Parameter Thermal Model	Stator & rotor temperature	Experimental PMSM data	0.94	4.10°C	Physics-based model; slower inference and limited adaptability
Nguyen et al. (2023) (Nguyen *et al.* 2023)	LSTM Network	Motor speed & torque	Industrial PMSM data	0.95	125 rpm	Effective for dynamic speed prediction, but higher inference time
Zhang et al. (2022) (Zhang *et al.* 2022)	1D-CNN	Motor speed	Simulated PMSM data	0.96	110 rpm	Good for speed prediction; no multi-target capability
Proposed Model (This Study)	Residual Dilated 1D-CNN	Motor speed, stator yoke & winding temp.	Real PMSM dataset	0.9969	101.89 rpm	Best accuracy across all targets; captures both short- & long-term dependencies efficiently

As shown in Table 5, prior studies such as Kirchgässner et al. (2021) (Kirchgässner *et al.* 2021) and Vansompel et al. (2014) (Vansompel *et al.* 2014) demonstrated strong performance in thermal prediction tasks, while Nguyen et al. (2023) (Nguyen *et al.* 2023) and Zhang et al. (2022) (Zhang *et al.* 2022) achieved competitive results in speed forecasting. However, these methods are either limited to a single target or require higher computational resources. In contrast, the proposed approach delivers high-accuracy multi-target predictions while maintaining computational efficiency, making it particularly suitable for real-time

PMSM monitoring, predictive control, and condition-based maintenance applications.

CONCLUSION

This study proposed a Residual Dilated One-Dimensional Convolutional Neural Network (1D-CNN) framework for short-horizon multi-target prediction of key Permanent Magnet Synchronous Motor (PMSM) operational parameters, namely motor speed, stator yoke temperature, and stator winding temperature. By combining dilated convolutions and residual connections, the model effectively captured both short- and long-term temporal dependencies while maintaining computational efficiency.

Experimental results demonstrated that the proposed model achieved exceptional predictive performance, with determination coefficients (R^2) exceeding 0.96 for all targets and an average R^2 of 0.9829. Low error values in Mean Squared Error (MSE), Root Mean Squared Error (RMSE), and Mean Absolute Error (MAE) metrics further validated the robustness of the approach.

Compared to conventional machine learning methods such as Gradient Boosted Regression Trees (GBRT) and Random Forests, as well as deep learning architectures like standard 1D-CNNs and LSTM-based models reported in the literature, the proposed framework consistently achieved higher accuracy while requiring less computational time for inference. The integration of dilated convolutions allowed for the efficient modeling of extended temporal dependencies without increasing parameter complexity, and residual connections ensured stable gradient flow, mitigating performance degradation in deeper architectures.

These advantages position the proposed framework as a strong candidate for real-time PMSM monitoring, predictive control, and condition-based maintenance applications, where early anomaly detection is crucial for safety, reliability, and operational efficiency. Future research will focus on expanding the dataset with additional operational parameters, validating the approach on various motor types, and exploring transfer learning and domain adaptation techniques to enhance generalization under diverse operating conditions.

Ethical standard

The authors have no relevant financial or non-financial interests to disclose.

Availability of data and material

The data that support the findings of this study are available from the corresponding author upon reasonable request.

Conflicts of interest

The authors declare that there is no conflict of interest regarding the publication of this paper.

Declaration of generative AI and AI-assisted technologies in the writing process

The authors declare that generative artificial intelligence (AI) tools were used during the preparation of this manuscript. Specifically, AI assistance was utilized for language editing, text refinement, and formatting purposes. The authors take full responsibility for the content and have carefully reviewed and verified all AI-assisted outputs.

LITERATURE CITED

Altmann, A., L. Toloşi, O. Sander, and T. Lengauer, 2010 Permutation Importance: A Corrected Feature Importance Measure. Bioinformatics **26**: 1340–1347.

Bai, S., J. Z. Kolter, and V. Koltun, 2018 An Empirical Evaluation of Generic Convolutional and Recurrent Networks for Sequence Modeling. arXiv preprint arXiv:1803.01271 .

Borovykh, A., S. Bohte, and C. W. Oosterlee, 2017 Conditional Time Series Forecasting with Convolutional Neural Networks. arXiv preprint arXiv:1703.04691 .

Bouziane, M., B. Bossoufi, A. Derouich, A. Lagrioui, M. Taoussi, *et al.*, 2024 Enhancing Temperature and Torque Prediction in PMSMs with BiLSTM. AIP Advances **14**: 105136.

Holtz, J. and M. U. I. Malik, 2006 Sensorless Detection of Rotor Position and Speed in Permanent-Magnet Synchronous Machines. IEEE Transactions on Industry Applications **42**: 1241–1248.

Jahns, T. M. and W. L. Soong, 1996 Pulsating Torque Minimization Techniques for Permanent Magnet AC Motor Drives – A Review. IEEE Transactions on Industrial Electronics **43**: 321–330.

Jing, H., Y. Chen, X. Zhao, and W. Sun, 2023 Gradient Boosting Decision Tree for Rotor Temperature Estimation in PMSMs. IEEE Transactions on Power Electronics **38**: 10617–10622.

Kaneko, H., 2022 Cross-Validated Permutation Feature Importance Considering Feature Correlation. Advanced Science **9**: e202200018.

Kim, L., 2025 Comprehensive Survey of Deep Learning for Time Series Forecasting. ACM Computing Surveys **57**: 1–37.

Kirchgässner, W., 2021 Electric Motor Temperature Dataset. Kaggle, Online.

Kirchgässner, W., O. Wallscheid, and J. Böcker, 2021 Estimating Electric Motor Temperatures with Deep Residual Machine Learning. IEEE Transactions on Power Electronics **36**: 7480–7488.

La Cava, W., J. T. Moore, B. D. Moore, P. Shankaranarayanan, and J. H. Moore, 2020 Interpretation of Machine Learning Predictions for Patient Outcomes Using Permutation Importance. IEEE Journal of Biomedical and Health Informatics **24**: 1414–1421.

LeCun, Y., Y. Bengio, and G. Hinton, 2015 Deep Learning. Nature **521**: 436–444.

Li, J. and T. Akilan, 2022 Global Attention-Based Encoder–Decoder LSTM for PMSM Temperature Prediction. IEEE Access **10**: 76921–76933.

Li, J., H. Huang, and T. Akilan, 2024 Data-Driven Temperature Prediction for PMSMs Using Deep Learning and Feature Selection. Energies **17**: 1234.

Liu, Z., T. Zhang, Y. Wang, and M. Xu, 2024 Hybrid Thermal Modeling with LPTN-Informed Neural Network for Multi-Node Temperature Estimation in PMSM. IEEE Transactions on Power Electronics Early Access.

Mi, X., Y. Zou, L. Zhu, L. Fang, and S. Ma, 2021 Permutation-Based Feature Importance Test (PermFIT) for Deep Neural Networks and SVMs. Bioinformatics **37**: 2633–2640.

Nguyen, T. T., T. H. Nguyen, and J. W. Jeon, 2023 Explicit Model Predictive Speed Control for Permanent Magnet Synchronous Motor with Torque Ripple Minimization. IEEE Access **11**: 134199–134210.

Pellegrino, L., A. Vagati, B. Boazzo, and P. Guglielmi, 2012 Performance Comparison Between Surface-Mounted and Interior PM Motor Drives for Electric Vehicle Application. IEEE Transactions on Industrial Electronics **59**: 803–811.

Pyrhönen, J., T. Jokinen, and V. Hrabovcová, 2014a *Design of Rotating Electrical Machines*. Wiley, Hoboken, NJ, USA, second edition.

Pyrhönen, J., A. Niemenmaa, and T. Jokinen, 2014b Thermal Be-

havior of Electrical Machines—An Overview. IEEE Transactions on Industrial Electronics **61**: 4391–4403.
Sheng, Y., X. Zhang, Z. Xu, and W. Guo, 2025 OLTEM: Lumped Thermal and Deep Neural Model for Temperature Estimation of PMSMs. Machines **13**: 57.
Tallam, R. M., T. G. Habetler, and R. G. Harley, 2002 Transient Model of Induction Machines with Stator Winding Turn Faults. IEEE Transactions on Industry Applications **38**: 632–637.
Thakur, D. and S. Kumar, 2024 Permutation Importance Based Modified Guided Regularized Random Forest for Feature Selection. Neurocomputing **517**: 372–383.
Vansompel, H., B. Sergeant, and L. Vandevelde, 2014 Lumped Parameter Thermal Model for a Permanent Magnet Synchronous Machine in a Hybrid Electric Vehicle. IEEE Transactions on Energy Conversion **29**: 823–831.
Vansompel, H., B. Sergeant, and L. Vandevelde, 2022 Thermal Management in PMSMs for Electric Vehicles: A Review. Energies **15**: 3210.
Winkler, A., M. Eisenbarth, and J. Andert, 2024 Physics-Informed Machine Learning for Electric Machine Thermal Management: A Review. IEEE Access **12**: 120050–120072.
Yu, F. and V. Koltun, 2015 Multi-Scale Context Aggregation by Dilated Convolutions. arXiv preprint arXiv:1511.07122 .
Zhang, P., Z. Liu, and M. Degano, 2021 Thermal Modeling and Analysis of Permanent Magnet Synchronous Motors for Electric Vehicle Applications. Energies **14**: 606.
Zhang, Y., M. Li, and K. Wang, 2022 Motor Speed Prediction of PMSMs Using One-Dimensional Convolutional Neural Networks. Energies **15**: 8423.
Zhu, Z. Q. and D. Howe, 2007 Electrical Machines and Drives for Electric, Hybrid, and Fuel Cell Vehicles. Proceedings of the IEEE **95**: 746–765.

How to cite this article: Aslan, E., Özüpak, Y., Alpsalaz, F. and Uzel, .H Accurate Short-Horizon Multi-Target Prediction of PMSM Operational Parameters via Residual Dilated 1D Convolutional Neural Networks. *Computational Systems and Artificial Intelligence*, 2(2),7-14, 2026.

ADBA
Computational Systems and Artificial Intelligence
Cutting-Edge Scientific Solutions

e-ISSN: 3108-4079
RESEARCH ARTICLE
Vol.2 / No.1 / 2026 / pp.15-20
https://doi.org/10.69882/adba.csai.2026013

A Comparative Analysis of Deep Reinforcement Learning Approaches in Symbolic Optimization Tasks: The Case of DQN, QT-Opt and Samuel

Cem Özkurt *,[1], **Ahmet Kutey Küçükler** *,[2], **Murat Karslıoğlu** *,[3] **and Ruveyda Nur Özdemir** *,[4]
*Department of Computer Engineering, Sakarya University of Applied Sciences, Sakarya, Turkiye.

ABSTRACT This study aims to comparatively analyze the performance of three reinforcement learning algorithms-DQN, QT-Opt, and Samuel's checkers algorithm-on the symbolic matrix multiplication task. The experiments were conducted using a customized simulation environment, MatrixMultiplyDiscoveryEnv, where each agent generates outer product-based symbolic actions to perform matrix multiplication with minimal error and computational cost. The reward function incorporates the Frobenius norm, operation count, and symbolic complexity. Based on 50,000 episodes, the QT-Opt algorithm demonstrated a highly stable reward profile, maintaining reward values close to zero throughout training. Samuel's algorithm showed rapid early learning, improving from -300 to around -100, but exhibited fluctuations in the later stages. In contrast, DQN's reward varied drastically, occasionally falling below -3000, indicating instability and sensitivity to environmental uncertainty. Regarding matrix error (Frobenius norm), Samuel's algorithm minimized its error to nearly zero in early training and maintained this performance. QT-Opt also performed well but showed occasional spikes in error. In terms of operation cost, QT-Opt consistently operated within 50-100 units, showing the highest efficiency. Samuel started with costs near 300, but reduced them gradually, converging towards QT-Opt's performance. DQN, however, showed wide and erratic cost distributions. In conclusion, QT-Opt achieved the most stable and efficient learning, particularly in continuous action domains. This paper provides a unique perspective by comparing classical and modern reinforcement learning methods within a unified experimental framework, highlighting both their historical significance and practical performance.

KEYWORDS
Reinforcement learning
QT-Opt
Symbolic optimization

INTRODUCTION

Reinforcement Learning (RL) is a powerful decision-making paradigm that enables an agent to discover optimal action policies based on reward signals through interaction with its environment. In this framework, three prominent methods in the literature, Deep Q-Network (DQN), QT-Opt, and Samuel's learning systems, are notable for their historical development, structural architecture, and application areas.

DQN was introduced by Mnih *et al.* (2015) and is one of the first deep reinforcement learning models that can make successful decisions in high-dimensional state spaces by integrating an experience repetition buffer and a target network structure. The theoretical foundation of DQN is later analyzed by Fan *et al.* (2020), who present the algorithmic convergence behavior and statistical error structure of this method. The contribution of mechanisms such as experience repetition and target network to success is theoretically justified. Furthermore, extended variants such as DQfD (Deep Q-learning from Demonstrations) developed by Hester *et al.* (2018) accelerate the learning process with human demonstrations, increasing the usability of DQN for real-world applications.

QT-Opt, developed by Kalashnikov *et al.* (2018), is a scalable and distributed deep reinforcement learning algorithm that achieves high success in continuous control problems such as robotic grasping based on visual inputs. In particular, based on closed-loop control logic, it allows the robot to dynamically update its grasping strategy with visual feedback. It achieved %96 grasping success with RGB camera data only. QT-Opt's high-parameter Q-function is characterized by its capacity to learn from MAP inference and real-world experiences.

From a historical perspective, Samuel (1959) checkers playing program is more than just a game analysis. It is the theoretical foundation for modern reinforcement learning approaches by incorporating value function estimation, heuristic search and self-play. Samuel's work demonstrates that a computer program can improve itself through experience, not just rules, and was among the first to use the term "machine learning".

This paper aims to comparatively analyze the three aforementioned methods DQN, QT-Opt and Samuel's learner systems in a single experimental and conceptual framework. DQN and QT-Opt,

Manuscript received: 22 November 2025,
Revised: 21 December 2025,
Accepted: 14 January 2026.

[1]cemozkurt@subu.edu.tr (**Corresponding author**).
[2]23010903094@subu.edu.tr
[3]24010903047@subu.edu.tr
[4]24010903035@subu.edu.tr

as contemporary deep learning-based reinforcement learning algorithms, are successful in high-dimensional and continuous action spaces. Samuel's method provides a historical reference point with its algorithmic simplicity and heuristic foundations.

In recent years, there has been a growing body of work in the literature analyzing DQN and QT-Opt either individually or in pairwise comparisons (Hester *et al.* 2018; Kalashnikov *et al.* 2018). However, comprehensive triple comparisons in which these methods are evaluated together from a historical and structural perspective are almost non-existent. In this context, our study aims to bring together classical and modern reinforcement learning approaches on the same ground, both to make the historical evolution visible and to empirically reveal the performance differences between the methods.

THEORETICAL REFERENCE

Reinforcement learning has emerged as an important paradigm for optimizing decision-making processes based on interaction with the environment in robotic systems. Over time, this field has evolved from classical algorithms to deep learning-based artificial intelligence systems. One of the most fundamental milestones in this evolution is Arthur Samuel's classical approach based on reinforcement learning principles. While Samuel's method offered a primitive learning process where decisions were shaped based on experience, today this structure has merged with deep structures capable of learning in multidimensional state and action spaces (Liao *et al.* 2024). Accordingly, modern algorithms built on Samuel's methodological foundations have reached the capacity to learn complex tasks with the contribution of big data and visual signals (Gao 2024).

The Deep Q-Network (DQN) algorithm is one of the revolutionary developments in the field of reinforcement learning. It is widely preferred in critical applications such as autonomous navigation and collision avoidance (AlMahamid and Grolinger 2025; Chen *et al.* 2024; de Sousa Bezerra *et al.* 2023), especially because it enables decision making under limited sensor data and high uncertainty environments. The advantage of DQN is that it can learn in continuous state spaces by modeling the Q-value function with a deep neural network. However, the classical DQN structure has certain limitations. To overcome these problems, variants such as Double DQN, Dueling DQN and Noisy DQN have been developed. These variants have produced effective results, especially in high-risk environments such as autonomous underwater vehicles and confined space robots(Al-Hamadani *et al.* 2024; Gao *et al.* 2023; Chen *et al.* 2024).

The integration of attention mechanisms into the DQN structure has further strengthened the mission success by increasing the environmental awareness of the system. Thanks to this integration, more responsive and adaptive solutions have been developed for collision avoidance missions in UAV systems (Al-Hamadani *et al.* 2024). DQN has also been shown to offer a satisfactory alternative in terms of robustness and information sharing in challenging tasks such as decentralized multi-robot control (Wu and Suh 2024). Thus, it provides a flexible basis for both the interaction of individual robots with the environment and the coordination of multi-agent systems.

The QT-Opt algorithm is another prominent approach, especially in tasks such as robotic arm manipulation with high-dimensional visual data. By combining value-based methods with policy optimization, QT-Opt makes the data collection process both safe and cost-effective thanks to its structure suitable for offline learning (Zhang *et al.* 2025). The integration of this algorithm with offline learning makes it easier for the robot to adapt to new situations by generalizing from previously observed data [16]. Especially in visual manipulation problems, high-performance policy learning can be achieved without directly interacting with the environment. In addition, recent work on behavior correction policies extends the safety boundaries of QT-Opt and ensures stable learning even in unsupervised scenarios (Dong *et al.* 2024).

The evolutionary impact of Samuel's classical method is not only of historical importance, but the principles derived from it are also evident in the design of modern artificial intelligence systems. For example, the integration of representation-based learning and DQN enables rapid adaptation to both static and dynamic conditions in tasks such as robotic arm control (Gao 2024). Such integrated structures not only improve task performance but also offer sustainable solutions for general AI architectures.

Multi-robot systems are another important application area of reinforcement learning. In these systems, real-time task sharing and coordination of agents with different abilities becomes quite complex with traditional methods, while multi-agent deep reinforcement learning approaches make this complexity manageable (Gao *et al.* 2023). In particular, the coordinated play of heterogeneous roles enables the system to perform adaptive task assignment and promotes collaborative learning (Pal *et al.* 2025). In addition, automatic task generation in task-diverse scenarios and learning reusable strategies for these tasks increase the scalability and flexibility of robotic systems (Jansonnie *et al.* 2024; Mao *et al.* 2023).

There are many studies in the literature where DQN and QT-Opt algorithms have achieved high performance on various robotic tasks. Samuel's method also provides a theoretical underpinning for these advanced algorithms, but comparative analysis of these methods in terms of performance, safety, sample efficiency and multi-task generalization within the same study is very limited. This paper presents a holistic view of the strengths and weaknesses of DQN, QT-Opt and Samuel methods from both theoretical and practical perspectives, especially in multi-tasking and high-risk robotic scenarios. Thus, it aims to provide a guiding reference for both academic and industrial applications.

MATERIALS AND METHODS

In this work, we use Deep Q-Network (DQN), QT-Opt and Arthur Samuel's checkers algorithm for reinforcement learning-based solutions to the symbolic matrix multiplication task. The experimental environment is based on the MatrixMultiplyDiscoveryEnv simulation environment designed to optimize symbolic processing efficiency. This environment vectorizes two input matrices and presents them to agents, which generate solutions through outer product-based symbolic actions. The reward function has a multi-component structure penalizing the Frobenius norm, number of operations and symbolic complexity. Model training is supported by classical and quantum critical architectures, and the algorithms are comparatively tested under the same conditions. DQN performed better in discrete action domains, while QT-Opt performed better in continuous action domains. Arthur Samuel's algorithm is included as a reference to establish historical context.

Data Set and Environment Definition

The experimental data set and the environment used in this study are based on an open-source reinforcement learning framework called Quantum Matrix RL. It is built on MatrixMultiplyDiscoveryEnv, a specialized simulation environment for the discovery of symbolic algorithms for basic linear algebra operations such

as matrix multiplication. The environment combines two input matrices $A \in \mathbb{R}^{n \times n}$ and $B \in \mathbb{R}^{n \times n}$ in a flattened form to generate an observation vector. The agent generates symbolic actions based on this observation. The agent's goal is to approximate the product $C = AB$ by multiplying the given matrices A and B with minimum number of operations and low symbolic cost. Actions defined in this environment represent symbolic operations such as low-rank outer product. Each action updates the agent's current estimate C_t. The reward function used as a feedback mechanism, $\|C_t - AB\|_2$ includes both an error metric based on the Frobenius norm and penalties for number of operations and symbolic complexity. Through this structure, the agent is incentivized to optimize not only accuracy but also computational efficiency.

The model training process is supported by classical or quantum-based critic structures. The data used in this study consists of the outputs of the models trained in simulation and allows the comparison of each algorithm under the same experimental conditions. Thus, the learning behavior of different reinforcement learning algorithms on symbolic optimization tasks can be objectively analyzed.

The DQN and QT-Opt algorithms are chosen for comparative analysis because they have different action space types. DQN is a classical method that is efficient in discrete action spaces and provides a strong foundation for discrete tasks such as symbolic matrix multiplication. On the other hand, the QT-Opt algorithm enables the exploration of more complex strategies thanks to its direct optimization capability in continuous action domains. These two methods provide meaningful counterexamples to evaluate the performance of different reinforcement learning paradigms in a common framework.

Furthermore, Arthur Samuel's checkers algorithm is included in the study as a historical reference. This method sheds light on the theoretical foundations of modern algorithms, especially with its value function-based learning approach, and provides an important perspective to contextualize the process of methodological evolution.

Deep Q-Network (DQN)

DQN combines classical Q-learning with deep neural networks to enable efficient learning in high-dimensional state spaces. The expected total reward (Q-value) of each state-action pair is estimated through a neural network. The learning process is based on minimizing the difference between the target Q-values and the predicted values based on the Bellman optimality equation.

$$L(\theta) = \mathbb{E}_{(s,a,r,s') \sim \mathcal{D}} \left[r + \gamma \max_{a'} Q_{\theta^-}(s', a') - Q_\theta(s, a) \right]^2 \quad (1)$$

In this formula, s represents the current state, a represents the action taken, r represents the immediate reward, s' represents the next state, a' represents the next possible actions, θ represents the parameters of the main network, θ' represents the fixed parameters of the target network and γ represents the discount coefficient chosen between 0 and 1. Experience replay memory and goal network techniques increase the stability of learning.

QT-Opt

QT-Opt performs policy learning through direct optimization in continuous action spaces. This method offers a more flexible and efficient solution space for continuous control problems that classical DQN has difficulty solving. Especially preferred in robotics applications, this method allows for the development of finer discriminative action strategies. Unlike DQN, in QT-Opt the optimal action is determined by choosing an argument that maximizes the Q-value.

$$a^* = \arg\max_a Q(s, a; \theta) \quad (2)$$

Where s is the current state, a is the feasible action, $Q(s, a; \theta)$ is the function that estimates the expected reward of the action in that state, and a^* is the action that maximizes this value. The QT-Opt algorithm also learns using Bellman-based target Q-values. This structure allows future reward expectations to be linked to present decisions.

$$y = r + \gamma \max_{a'} Q_{\theta^-}(s', a'; \theta^-) \quad (3)$$

Where y is the target Q-value, r is the immediate reward, $s'$is the next state, a' is the possible next actions, γ is the discount coefficient, and $Q(s', a'; \theta-)$ is the Q-value estimated with the target network parameters. QT-Opt balances exploration and exploitation in action selection with strategies such as ϵ-greedy.

Arthur Samuel's Checkers Algorithm

Samuel's algorithm is an early example of value function-based learning. This approach was one of the first systems to allow a computer to learn its own strategies by playing games. This model laid the foundations for traditional AI applications and played a key role in the historical development of modern reinforcement learning algorithms. The system evaluates each game state with a weighted sum of certain features.

$$V(s) = \sum_i w_i \, x_i(s) \quad (4)$$

In this formula, $x_i(s)$ defines the ith attribute of the state (e.g. number of pieces, position, etc.), w_i is the weight assigned to this attribute, and $V(s)$ is the total score of the state. The learning process is performed by updating these weights based on game experience. This structure makes it possible to make sense of previously unseen situations through generalizable evaluation functions.

RESULTS AND DISCUSSIONS

In this section, the performance of DQN, QT-Opt and SAMUEL algorithms over 50,000 episodes is analyzed comparatively according to three main criteria: reward, matrix error (Frobenius norm) and operational cost. The findings are analyzed in detail with graphs.

Reward Evaluation

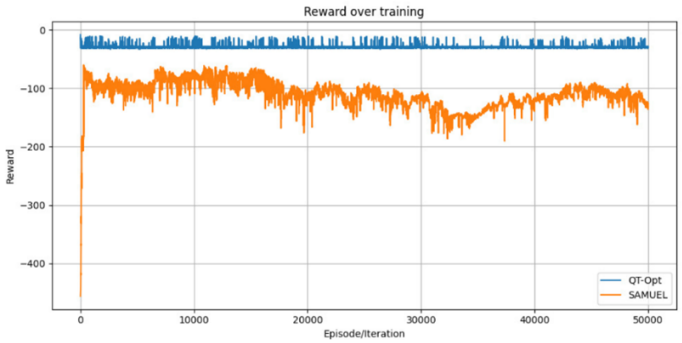

Figure 1 QT-Opt and SAMUEL Reward Over Training

As can be seen in Figure 1, the QT-Opt algorithm has a very stable reward profile throughout the training process and these values are generally close to zero. This shows that QT-Opt makes very stable and reliable decisions in the applied environment. SAMUEL, on the other hand, rises rapidly from negative values in the early stages and then fluctuates around -100. This shows that SAMUEL reaches a certain performance limit in the learning process, but it is not as stable as QT-Opt.

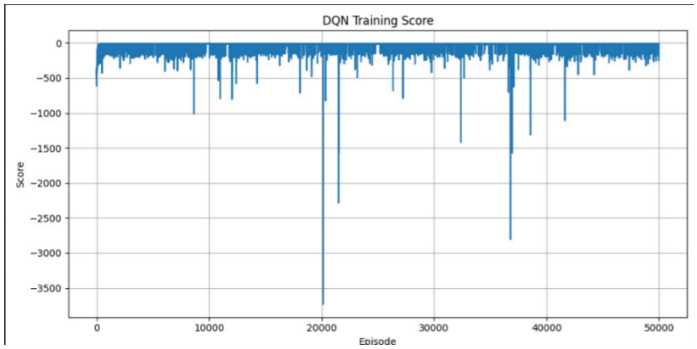

Figure 2 DQN Training Score

As seen in Figure 2, when the DQN algorithm is examined, it is seen that the performance is quite variable and there are serious performance losses that sometimes fall below -3000. This high variance shows that the model has difficulty learning a stable policy and is not robust against environmental uncertainties.

Matrix Error (Frobenius Norm)

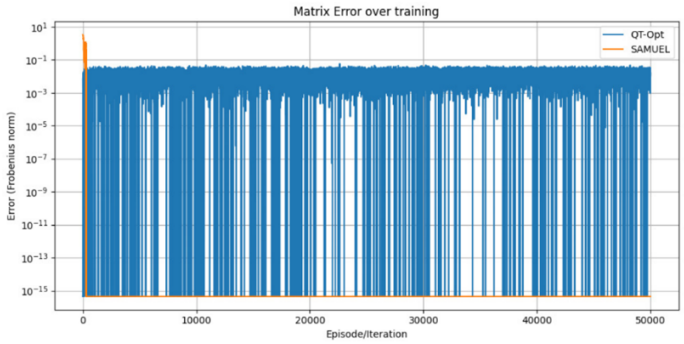

Figure 3 QT-Opt and SAMUEL Matrix Error Over Training

As seen in Figure 3., when evaluated in terms of matrix error values, the SAMUEL algorithm has demonstrated a remarkable success. It minimized its error at the beginning of the training process and reached almost zero levels and maintained this stable structure throughout the training period. Although QT-Opt tries to keep its error at low levels with relatively high frequency fluctuations, sudden jumps in these values indicate instability in the learning process.

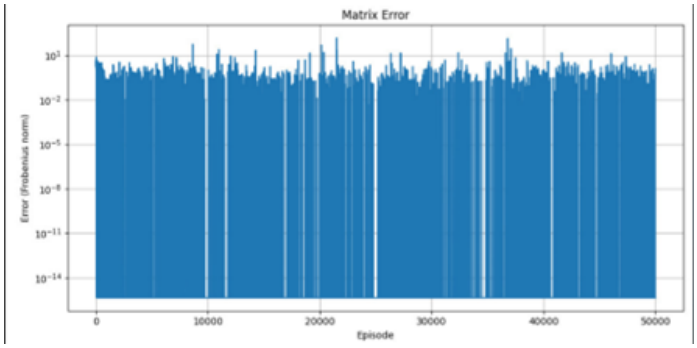

Figure 4 DQN Matrix Error

As seen in Figure 4., it is observed that in the DQN algorithm, the errors are constantly changing and reach very high values in certain sections. This shows that the algorithm cannot fully provide numerical stability in weight updates and therefore does not converge stably.

Operation Cost Analysis

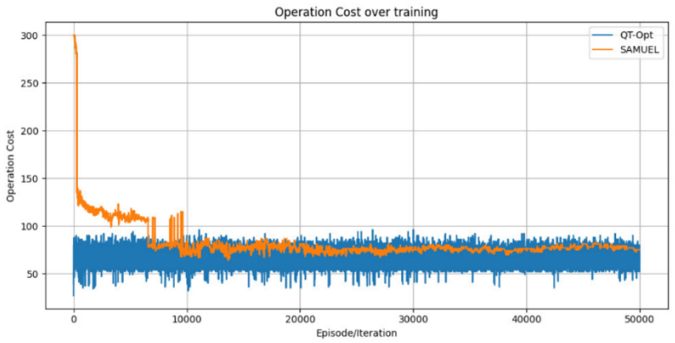

Figure 5 QT-Opt and SAMUEL Operation Cost Over Training

As seen in Figure 5, the QT-Opt algorithm exhibits a very successful performance in terms of operational costs. During most of the training, costs fluctuated between 50 and 100 units, and this fluctuation remained low amplitude. Although the SAMUEL algorithm started with high costs at the level of 300 at the beginning, it managed to reach a performance close to QT-Opt by systematically reducing its costs in the following sections. This reveals SAMUEL's long-term learning success and adaptability.

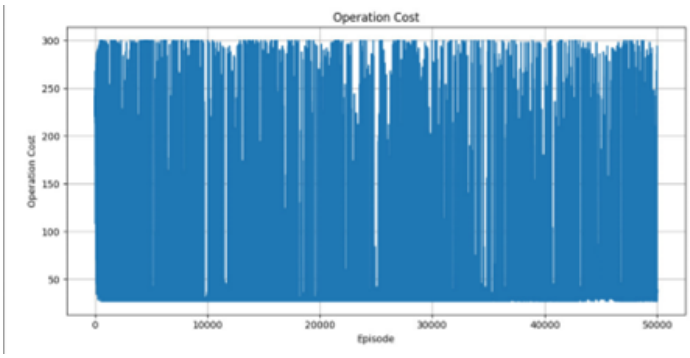

Figure 6 DQN Operation Cost

As seen in Figure 6, the operating costs of the DQN algorithm show an extremely irregular and wide distribution. Serious jumps and fluctuations were observed during the training period; this shows that the model could not achieve permanent and sustainable learning in terms of cost reduction.

In this study, the effect of the Cross Entropy method on three different reinforcement learning algorithms (DQN, QT-Opt and Samuel) was comparatively analyzed. The findings revealed that the QT-Opt algorithm, in particular, outperformed the other methods in terms of both reward stability and processing efficiency. This result is consistent with the findings of Kalashnikov et al., which showed that the closed-loop control structure proposed for QT-Opt can increase comprehension success up to 96% in high-dimensional visual tasks (Kalashnikov *et al.* 2018).

Another remarkable advantage of QT-Opt is its ability to achieve high success with offline learning. In the study of Wei et al., it was reported that significant improvements were achieved in learning processes by integrating advanced derivatives of DQN (NoisyNet, PER, Distributional DQN) into the QT-Opt structure (Wei *et al.* 2023). In our study, Frobenius norm and operational cost metrics showed that QT-Opt works more balanced and with low errors. It is reported in the literature that advanced optimization contributions, such as the QT-Opt-PSO integration proposed by Zhang *et al.* (2025), similarly enhance error reduction.

On the other hand, the performance of the DQN algorithm is lower than QT-Opt due to the high variance reward profile and fluctuating matrix errors. This situation confirms the basic requirement of the improved DQN algorithms proposed by Chen et al. for indoor obstacle avoidance problems. Also, the Agile DQN architecture proposed by AlMahamid and Grolinger improved the performance of DQN under partial observations with attention mechanisms and timing-sensitive Q-estimation strategies (Gao 2024; Chen *et al.* 2024). Such improved architectures are promising to overcome the limitations of classical DQN, especially in scenarios with high visual complexity (e.g. UAV obstacle avoidance). In particular, the stability of DQN has been tried to be increased with the PER-D2MQN structure, and in this direction, it has been observed in our study that the classical DQN architecture is not robust to environmental uncertainties.

Additionally, as suggested by (Liao *et al.* 2024), combining Dueling and Noisy DQN architectures can increase success rates, especially in complex environment conditions (e.g., autonomous underwater vehicles), but such DQN variants have limited applicability in our experimental setting since they require more complex and computationally intensive systems than the original DQN structure (Liao *et al.* 2024). In this context, DQN has been shown to have room for improvement in terms of sample efficiency and learning stability.

Samuel's checker algorithm, with its low level of complexity and intuitive decision structure, showed a tendency for rapid learning, especially at the beginning of the training period. However, performance instability in the medium and long term and limited adaptation capacity limits the use of this method in modern tasks. However, as Sutton and Barto emphasize, Samuel's value function-based approach constitutes the conceptual origin of today's deep value-based systems and continues to be a source of inspiration (Sutton and Barto 1998).

As a result, Cross Entropy based optimization produces more efficient results in QT-Opt, which shows that this algorithm performs more effective and stable learning in continuous action spaces. Future studies can test the applicability of this method in multi-agent systems and representation-based learning scenarios, and hybridization of QT-Opt with current variants of DQN may offer new balance points between sample efficiency and computational cost (Wu and Suh 2024; Al-Hamadani *et al.* 2024).

Acknowledgments

The authors would like to thank Sakarya University of Applied Sciences Arifical Intelligence and Data Science Application and Research Center for supporting this study.

Ethical standard

The authors have no relevant financial or non-financial interests to disclose.

Availability of data and material

The data that support the findings of this study are available from the corresponding author upon reasonable request.

Conflicts of interest

The authors declare that there is no conflict of interest regarding the publication of this paper.

Declaration of generative AI and AI-assisted technologies in the writing process

The authors declare that generative artificial intelligence (AI) tools were used during the preparation of this manuscript. Specifically, AI assistance was utilized for language editing, text refinement, and formatting purposes. The authors take full responsibility for the content and have carefully reviewed and verified all AI-assisted outputs.

LITERATURE CITED

Al-Hamadani, M. N., M. A. Fadhel, L. Alzubaidi, and B. Harangi, 2024 Reinforcement learning algorithms and applications in healthcare and robotics: A comprehensive and systematic review. Sensors **24**: 2461.

AlMahamid, F. and K. Grolinger, 2025 Agile dqn: Adaptive deep recurrent attention reinforcement learning for autonomous uav obstacle avoidance. Scientific Reports **15**: 1–18.

Chen, C., J. Yu, and S. Qian, 2024 An enhanced deep q-network algorithm for localized obstacle avoidance in indoor robot path planning. Applied Sciences **14**: 11195.

de Sousa Bezerra, C. D., F. H. T. Vieira, and D. P. Q. Carneiro, 2023 Autonomous robotic navigation approach using deep q-network late fusion and people detection-based collision avoidance. Applied Sciences **13**: 12350.

Dong, Q., T. Kaneko, and M. Sugiyama, 2024 An offline learning of behavior correction policy for vision-based robotic manipulation. In *Proceedings of the IEEE International Conference on Robotics and Automation*, pp. 5448–5454.

Fan, J., Z. Wang, Y. Xie, and Z. Yang, 2020 A theoretical analysis of deep q-learning. In *Proceedings of Learning for Dynamics and Control*, pp. 486–489.

Gao, T., 2024 Optimizing robotic arm control using deep q-learning and artificial neural networks through demonstration-based methodologies: A case study of dynamic and static conditions. Robotics and Autonomous Systems **181**: 104771.

Gao, Y., J. Chen, X. Chen, C. Wang, J. Hu, *et al.*, 2023 Asymmetric self-play-enabled intelligent heterogeneous multirobot catching system using deep multiagent reinforcement learning. IEEE Transactions on Robotics **39**: 2603–2622.

Hester, T., M. Vecerik, O. Pietquin, M. Lanctot, T. Schaul, *et al.*, 2018 Deep q-learning from demonstrations. In *Proceedings of the AAAI Conference on Artificial Intelligence*, volume 32.

Jansonnie, P., B. Wu, J. Perez, and J. Peters, 2024 Unsupervised skill discovery for robotic manipulation through automatic task generation. In *Proceedings of the IEEE-RAS International Conference on Humanoid Robots*, pp. 926–933.

Kalashnikov, D., A. Irpan, P. Pastor, J. Ibarz, A. Herzog, *et al.*, 2018 Scalable deep reinforcement learning for vision-based robotic manipulation. In *Proceedings of the Conference on Robot Learning*, pp. 651–673.

Liao, X., L. Li, C. Huang, X. Zhao, and S. Tan, 2024 Noisy dueling double deep q-network algorithm for autonomous underwater vehicle path planning. Frontiers in Neurorobotics **18**: 1466571.

Mao, J., T. Lozano-Pérez, J. B. Tenenbaum, and L. P. Kaelbling, 2023 Learning reusable manipulation strategies. In *Proceedings of the Conference on Robot Learning*, pp. 1467–1483.

Mnih, V., K. Kavukcuoglu, D. Silver, A. A. Rusu, J. Veness, *et al.*, 2015 Human-level control through deep reinforcement learning. Nature **518**: 529–533.

Pal, A., A. Chauhan, and M. Baranwal, 2025 Together we rise: Optimizing real-time multi-robot task allocation using coordinated heterogeneous plays. arXiv preprint arXiv:2502.16079.

Samuel, A. L., 1959 Some studies in machine learning using the game of checkers. IBM Journal of Research and Development **3**: 210–229.

Sutton, R. S. and A. G. Barto, 1998 *Reinforcement Learning: An Introduction*. MIT Press, Cambridge, MA, USA.

Wei, S., C. Li, J. Seyler, and S. Eivazi, 2023 Integration of efficient deep q-network techniques into qt-opt reinforcement learning structure. In *Proceedings of the International Conference on Agents and Artificial Intelligence*, volume 3, pp. 592–599.

Wu, B. and C. S. Suh, 2024 Deep reinforcement learning for decentralized multi-robot control: A dqn approach to robustness and information integration. In *Proceedings of the ASME International Mechanical Engineering Congress and Exposition*, volume 88636, p. V005T07A035.

Zhang, H., S. Zeng, Y. Hou, H. Huang, and Z. Xu, 2025 Improved qt-opt algorithm for robotic arm grasping based on offline reinforcement learning. Machines **13**: 451.

How to cite this article: Özkurt, C., Küçükler, A. K., Karslıoğlu, M. and Özdemir, R. N. A Comparative Analysis of Deep Reinforcement Learning Approaches in Symbolic Optimization Tasks: The Case of DQN, QT-Opt and Samuel. *Computational Systems and Artificial Intelligence*, 2(3),15-20, 2026.

ADBA
Computational Systems and Artificial Intelligence
Cutting-Edge Scientific Solutions

e-ISSN: 3108-4079
RESEARCH ARTICLE
Vol.2 / No.1 / 2026 / pp.21-32
https://doi.org/10.69882/adba.csai.2026014

On the Fractional-Order Derivative Effects on the ABS Robust Control Performance

Emery Baroki Munphano [*,1], **Kammogne Soup Tewa Alain** [α,2], **Eloi Jean Jacques Blampain** [β,3] **and Cédric Tolonang Noufozo** [§,4]

[*,β]Unity of physical Research (URPhy), Laboratory – Materials, Components and Signals P.O. Box 901, Franceville – Gabon, University of Sciences and Techniques of Masuku_Franceville, Gabon, [*,α,§]Research Unit of Condensed Matter Electronics and Signal Processing (URMACETS), University of Dschang, Cameroon, [*]Department of Electrotechnics, Higher Pedagogy and Technique of Goma, (ISPT/Goma), DR Congo.

ABSTRACT This study conducts a comparative analysis of sliding mode control (SMC) and fractional-order sliding mode control (FOSMC) for application in antilock braking systems (ABS). Based on foundational principles of theoretical mechanics, the ABS dynamics are modeled as a single-input system to analyze wheel-slip regulation under diverse and variable road conditions. Both the conventional SMC and the proposed FOSMC are designed using a Lyapunov-based approach to ensure robust stability, with the latter incorporating fractional-order derivatives to refine the sliding surface and dynamic response. The conventional SMC method, while demonstrating strong robustness and disturbance rejection capabilities, is found to induce persistent chattering during transient phases, which can compromise system reliability and actuator longevity. By contrast, the FOSMC controller enhances transient behavior by attenuating chattering and yielding smoother, more consistent wheel-slip tracking. The inclusion of fractional-order terms contributes to faster convergence and improved adaptation to abrupt changes in road friction, though it introduces increased computational complexity. Numerical simulations validate the performance of both controllers across multiple driving scenarios, including dry, wet, and icy road conditions. Results confirm that FOSMC significantly reduces chattering, accelerates system convergence, and maintains stable braking performance with greater consistency compared to conventional SMC, establishing its potential for implementation in advanced ABS designs.

KEYWORDS
Antilock braking system
Sliding mode control
Fractional order control
Robust control

INTRODUCTION

Since the introduction of the automobile, the importance of safety in trajectory control, particularly regarding braking systems, has been widely recognized. This has led to the development of innovative safety systems capable of preventing wheel lock during sudden or heavy braking, thereby maintaining tire traction and steering ability, such as antilock braking systems (ABS) (Pretagostini *et al.* 2020). Depending on the types of actuators used, there are three braking modes: hydraulic friction braking (HFB), hybrid braking, and electric motor braking (EMB). However, hydraulic friction braking is the most commonly employed method due to its efficiency and reliability (Pretagostini *et al.* 2020). ABS technology is specifically designed to adjust braking pressure, ensuring wheel slip remains within a range of 10% to 20% (Gowda and Ramachandra 2017). This optimization maximizes braking force while maintaining the lateral steering force necessary for directional control. To design effective ABS controllers, comprehending vehicle dynamics and wheel slip behavior is essential (Jazar 2008; Geleta *et al.* 2023).

During braking, the interaction between a vehicle's wheels and the road surface produces tractive forces , which can be quantified as the product of the road coefficient and vertical forces . This coefficient can be expressed as a function of wheel slip . In ABS, the challenge lies in setting a desired wheel slip ratio that reflects the difference between wheel velocity and road velocity. Therefore, the primary objective of ABS design is to maintain the slip ratio as close as possible to the optimal value of 0.2, where tractive force is maximized (Chen *et al.* 2022). This condition is critical for effective braking, as achieving a slip ratio of zero is not feasible. ABS represents a significant advancement in automotive active safety, aimed at preserving vehicle stability and maneuverability during emergency braking by preventing wheel lock. The major challenge arises from the inherent nonlinearity and uncertainties in the vehicle-tire-road dynamic model. The design of ABS control faces substantial uncertainties related to variations in road grip, vehicle load, and tire properties (Chen *et al.* 2022). To tackle these challenges, extensive research has been directed toward optimizing wheel slip control, a key parameter for enhancing system efficiency and robustness (Zhao *et al.* 2024).

Manuscript received: 19 November 2025,
Revised: 27 December 2025,
Accepted: 4 January 2026.

[1]iremrbar@gmail.com
[2]kouaneteoua@yahoo.fr (**Corresponding author**)
[3]eloiblampain@gmail.com
[4]noufozo3285@gmail.com

Classical controllers, such as bang-bang and PID controllers, have been proposed and calibrated for specific road conditions but often exhibit inefficiency and instability during braking (Nemah 2018). Various studies in braking control have explored sliding mode control (SMC) methods (Bi *et al.* 2024). For instance, researchers have proposed control strategies for ABS based on vehicle longitudinal dynamics (Schinkel and Hunt 2002). However, limitations in these nonlinear models sometimes fail to capture the intricate dynamics of real-world vehicle behavior on diverse surfaces. Consequently, the performance of proposed controllers can vary based on specific vehicle parameters and road configurations, and chattering remains a significant issue in SMC implementations. Several researchers have focused on minimizing chattering, a prominent feature of SMC systems. For example, algorithms for ABS have been developed comparing the Lyapunov-based sliding mode controller (LSMC) and the reaching-law-based sliding mode controller (RSMC) (Chereji *et al.* 2021), which show robust performance in managing uncertainties with fewer tuning parameters. Despite their promise, limitations persist. The models employed are often simplified and may not fully account for the complexities of real-world conditions, where uncertainties can fluctuate significantly. While these algorithms aim to streamline computational complexity, their effectiveness can still be sensitive to parameter adjustments, and they may not adequately address vibration issues that could affect user comfort and system longevity. Moreover, most validations have taken place in controlled settings, which may not accurately reflect real driving situations, raising questions about the scalability of these controllers in more complex systems.

To address the nonlinearities and uncertainties inherent in Antilock Braking System (ABS) frameworks, along with the challenges posed by chattering in sliding mode control, a robust control strategy has been developed to enhance the braking system's resilience against disturbances (Garcia Torres *et al.* 2022; Khadr *et al.* 2024). Recent advancements have introduced methods that leverage fuzzy logic to estimate the road adhesion coefficient, facilitating real-time optimization of slip rates (Gengxin *et al.* 2022). Evaluating these methods against traditional control strategies, such as PID, has yielded significant improvements in braking distance and response times, ultimately enhancing safety (Latreche and Benaggoune 2015). Nonetheless, the simplified models employed may inadequately capture the wide spectrum of road conditions, and the accuracy of adhesion coefficient estimations can be compromised by unmodeled uncertainties. Additionally, the sensitivity to parameter variations and potential chattering issues within sliding mode controllers can negatively impact overall performance. Recently, Sina et al., proposed an innovative control system that incorporates fuzzy logic control (FLC) to effectively mitigate issues related to nonlinearity, uncertainties, and disturbances, without the need for human intervention during braking. They introduced an adaptive fuzzy sliding mode longitudinal control strategy tailored for vehicles with ABS, aimed at minimizing braking distances (Namaghi and Moavenian 2019; Abdul Zahra and Abdalla 2020; Max *et al.* 2021). Concurrently, neural network control (NNC) has emerged as a complementary approach, with work by Sebanovic et al. developing artificial neural networks designed for real-world data-driven virtual sensors in vehicle suspension systems. Their research includes applications such as neural network-based model reference control for electric vehicle braking and multi-task learning driven by deep graph neural networks (Sabanovic *et al.* 2024; Vodovozov *et al.* 2021; Xiao 2022). While these methodologies exhibit promising performance, their design and implementation can be complex and resource-intensive. Researchers continue to refine control designs to bolster braking controller robustness through established mathematical frameworks. Researchers have designed controllers that regulate wheel slip to desired values by combining sliding mode control with fractional calculus (Tang *et al.* 2013). It for the great importance to recall that many works presented in littérature consider the interger ABS which make the performance of the controllers questionable in real time. With the ABS fractional order consideration, the dynamic models used for ABS may oversimplify the intricate variables affecting vehicle behavior during braking, which can impede the adaptive controller's ability to accurately estimate uncertainties encountered in real-world conditions, potentially degrading system performance. Additionally, vibration issues commonly linked to sliding mode controllers may not be fully resolved, adversely affecting user comfort and system durability. The fractional ABS aim to maintain robustness against external disturbances, featuring a dynamic fractional order sliding surface that enhances both response speed and controller flexibility.

This study systematically investigates two primary control methodologies: classic sliding mode control (CSMC) and fractional order sliding mode control (FOSMC). Comparing these methods is crucial for illuminating their respective performances and advantages. A clear presentation of these comparisons is necessary, supported by a concise table detailing the performance metrics of each method. Importantly, fractional order modeling in ABS offers enhanced control flexibility compared to its integer-order counterparts, making it a central focus of this research. To address existing gaps in the literature, this study carefully compares CSMC and FOSMC, specifically underscoring slip ratio regulation in ABS. Among the benefits of FOSMC is its advanced modeling capability, which facilitates better adaptability to parametric variations and external disturbances. The integration of fractional-order differential operators improves the dynamics of the sliding surface, resulting in faster convergence and greater robustness of the controller. Despite these advantages, comprehensive comparisons of CSMC and FOSMC within the ABS framework, accounting for realistic disturbances such as variations in road adhesion and sensor noise, are still limited. Consequently, this research aims to quantify the contributions of fractional order modeling in terms of tuning flexibility and chattering reduction, while also evaluating performance enhancements in slip regulation, stopping distance, and convergence time in comparison to classical benchmarks like integer-order sliding mode control.

This paper focuses primarily on constant actuator disturbances and modelling uncertainties, highlighting their impact on vehicle longitudinal dynamics, particularly during braking. It proposes a robust controller based on a fractional-order sliding mode to address these challenges compared to the conventional sliding mode. Among the disturbances mentioned are variations in vehicle mass, wheel radius and wheel inertia, which can influence the system. The design presented aims to manage the longitudinal dynamics of vehicles in the context of ABS system. We take into account constant actuator disturbances and modelling uncertainties, which vary depending on road conditions. These disturbances, such as brake pad wear, can cause a lag between the control output and the actuator response, compromising braking performance. In addition, variations in vehicle parameters and road surface conditions can affect the coefficient of friction and, consequently, stability during braking. In response to these challenges, the paper proposes a robust controller capable of maintaining the desired slip trajectory despite uncertainties. Using Lyapunov theory, the controller ensures system stability in a dynamic setting, taking into

account various scenarios, including actuator failures. Simulations show that the fractional-order controller outperforms traditional controllers, ensuring accurate and rapid tracking of reference values under normal conditions as well as in the presence of model variations or failures. This approach highlights the importance of robust design for active vehicle safety systems.

To bridge this gap, this paper presents a comparative study between classic sliding mode control and fractional order sliding mode control for robust controller design in anti-lock braking systems. The principal contributions of this work are as follows:

- Design of classical and fractional order sliding mode control laws using a quarter-vehicle model that incorporates fractional-order dynamics.
- A rigorous stability analysis base on Lyapunov function adapted to fractional-order systems.
- Comprehensive numerical validation across diverse operating conditions (dry asphalt, concrete, snow, and ice), with evaluation of performance indices such as ITAE and ITE.
- Presentation of a performance summary table highlighting improvements offered by the fractional-order approach, especially in the presence of unmodeled disturbances.

The remainder of this paper is organized as follows: Section 2 details the classic sliding mode control using a quarter-vehicle model and problem formulation. Section 3 presents the design and stability proof of the proposed controller. Section 4 discusses the simulation results and performance analysis, and Section 5 provides concluding remarks.

CLASSIC SLIDING MODE CONTROL FOR ABS

The dynamics of the antilock braking system (ABS) can be defined as the collection of behaviors and responses of a vehicle's braking system, influenced by various parameters such as vehicle speed, tire grip on the road, and the forces applied during braking, Fig. 1.

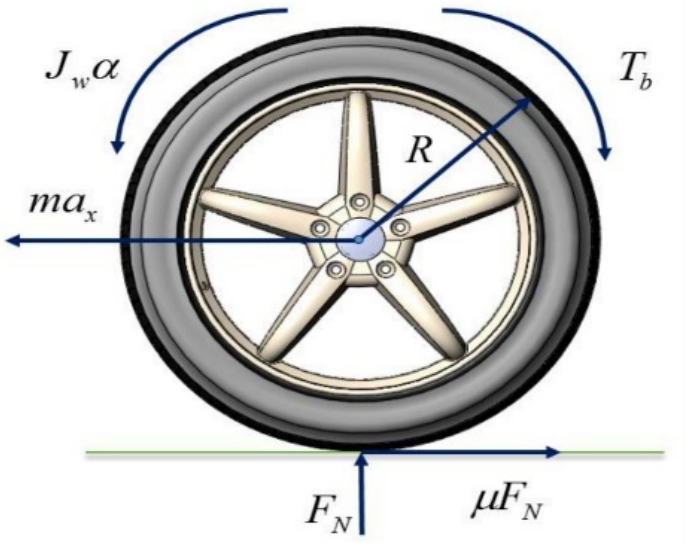

Figure 1 The antilock braking system model diagram

The vehicle wheel is equipped with a disk braking system. The diagram below illustrates the dynamics of a wheel, showing key components such as torque T_b , angular acceleration , moment of inertia J_ω, linear acceleration a_x, normal force F_N, and frictional force $\mu(F_N)$ (Abdul Zahra and Abdalla 2020). The torque applied to the wheel induces angular acceleration, while the moment of inertia determines the resistance to changes in rotation. The linear acceleration reflects the wheel's forward motion, influenced by the frictional force that enables grip on the road. These interactions are governed by Newton's laws (Garcia Torres *et al.* 2022; Abdul Zahra and Abdalla 2020). Understanding these dynamics is crucial for systems like anti-lock braking systems (ABS), ensuring vehicle stability and preventing wheel lock-up during braking. The normal force $F_z = mg$ refers to the perpendicular force exerted by the road surface on the wheels of a vehicle, Fig. 1. This force is crucial as it directly influences tire grip and braking performance, with m the mass of the vehicle. F_x is the road longitudinal friction force, which can be given by the coulomb law ;

$$F_x = \mu(\lambda)F_N \tag{1}$$

The road coefficient of adhesion μ, depends on many factors including tire-road condition. The wheel velocity and the value of wheel slip λ is defined as follow:

$$\lambda = \frac{v_x - r_w}{v_x} \tag{2}$$

with

$$\dot{\lambda} = -((1\lambda)/(mv_x) + r^2/(Jv_x))\mu F_N + r/(Jv_x)T_B \tag{3}$$

The wheel slip lies in [0,1]. If $\lambda = 0$, it indicates that the wheel and vehicle velocities are the same, if $\lambda = 1$, it indicates that the wheel is locked up. Table 1 shows the friction model parameters for various road surfaces.

Table 1 Friction model parameters for different road conditions

Surface_conditions	C1	C2	C3
Dry asphalt	1.2801	23.99	0.52
Wet asphalt	0.857	33.822	0.347
Dry concrete	1.1973	25.168	0.5373
Snow	0.1946	94.129	0.0646
Ice	0.05	306.39	0.000

The tire friction model is a nonlinear static function of several physical variables such as wheel slip and vehicle velocity, Fig. 2. In this paper, the tire friction model introduced by Burckhardt isused. The model is as follows:

$$\mu(\lambda, v_x) = C_1(1 - e^{-C_2\lambda}) - C_3\lambda \tag{4}$$

Where C_1 is the maximum value of friction curve, C2 is the friction curve shape and C3 is the friction curve difference between the maximum value and the value corresponding to $\lambda = 1$.

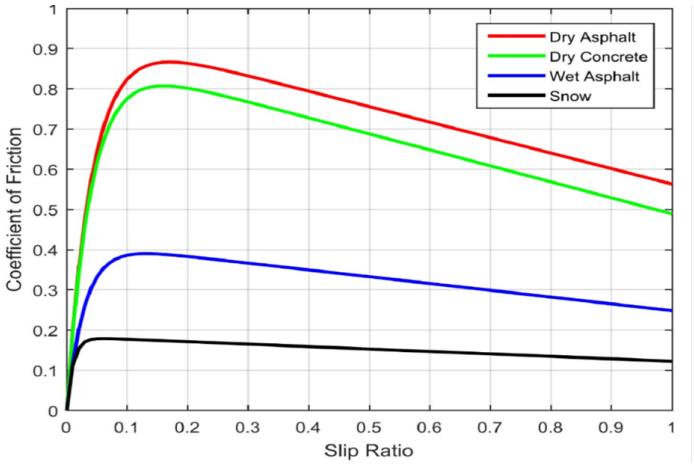

Figure 2 Coefficients of road friction versus wheel slip ratio

System formulation

In this section, a classic sliding mode controller is proposed for the ABS. The control objective is to find a control law so that the slip can track the desired trajectory λ_d. Define the tracking error as follows:

$$e = \lambda_d - \lambda \tag{5}$$

The first step is the choice of a suitable sliding surface Eq. (4).

$$s = \dot{e} + k_1 e \tag{6}$$

where k_1 denotes a positive constant, gain of robustness. From the Eq. (4) we define the time derivation of s ;

$$\dot{s} = \ddot{e} + k_1 \dot{e} \tag{7}$$

The new fast terminal dynamic sliding surface is chosen as:

$$\zeta = s + k_2 s + k_3 \int s^{(p/q)} dt \tag{8}$$

Where k_2, p and q are positive constants and $p \succ q \in Z$. By substituting Eqs. (3) and (5) into Eq. (8) yields:

$$\begin{aligned} \dot{\zeta} = -\dot{\lambda} + k_2 \Bigg[-\ddot{\lambda} - k_1 \left(\frac{1-\lambda}{m v_x} + \frac{r^2}{J v_x} \right) \\ \mu F_N - k_1 \frac{T_b R}{J v_x} + k_3 (-\dot{\lambda} - k_1 e)^{p/q} \end{aligned} \tag{9}$$

Considering the constraint $\dot{\zeta} = 0$, torque of the control can be obtained as follows:

$$\begin{aligned} T_b = \frac{J v_x}{r} \Bigg[\left(\frac{\mu F_N - \lambda}{m v_x} + \frac{\mu F_N r}{J v_x} \right) - \frac{\dddot{\lambda}}{k_1 k_2} \\ - \frac{\ddot{\lambda}}{k_1} + \frac{k_3}{k_1 k_2} (-\dot{\lambda} - k_1 e)^{p/q} + k_{11} \mathrm{sgn}(\zeta) \Bigg] \end{aligned} \tag{10}$$

where the switch gain k_{11} is a positive, and

$$\mathrm{sgn}(\zeta) = \begin{cases} +1, & \zeta \succ 0 \\ 0 & \zeta = 0 \\ -1 & \zeta \prec 0 \end{cases} \tag{11}$$

Substituting Eq. (9) into (10) results in:

$$\dot{\zeta} = -2\dddot{\lambda} - \ddot{\lambda} - k_1 k_2 k_{11} \mathrm{sgn}(\zeta) \tag{12}$$

It should be noted that the acceleration parameters $a_p = -2\dddot{\lambda} - k_2 \ddot{\lambda}$ compensates the controller torque T_b. Therefor the Eq. (12) can be expressed as follows:

$$\dot{\zeta} = -k_1 k_2 k_{11} \mathrm{sgn}(\zeta) \tag{13}$$

Theorem 1: If the control law (10) is applied to the wheel slip dynamics (8), the wheel slip trajectory will converge to the newly defined surface in (12). Consequently, the traction error (7) will diminish to zero in a finite time.

Proof: Considering the candidate Lyapunov function,

$$V = |\zeta| \tag{14}$$

The derivative of Eq. (14) leads to

$$\dot{V} = \dot{\zeta} \zeta \tag{15}$$

Therefore,

$$\dot{V} = \dot{\zeta} sgn(\zeta) \tag{16}$$

Substitution of Eq. (13) into Eq. (16) results in

$$\dot{V} = -k_1 k_2 k_{11} \mathrm{sgn}(\zeta)^2 \leq 0 \tag{17}$$

The tracking error decays to zero if the SMC parameters and k_1,k_2, k_3 and $k_1 1$ are chosen appropriately. Eq. (30) can be rewritten as:

$$\dot{V} = \frac{d\zeta}{dt} - k_1 k_2 k_{11} \tag{18}$$

From Eq. (18) we have the finite time of convergence;

$$dt = \frac{d|\zeta|}{-k_1 k_2 k_{11}} \tag{19}$$

Taking integral of both sides of Eq. (19) from t=0 to t_f;

$$\int_0^{t_f} dt = \int_{|\zeta(0)|}^{|\zeta(t_f)|} \frac{d|\zeta|}{-k_1 k_2 k_{11}} \tag{20}$$

By setting $\zeta(t_f) = 0$ and the finite time of convergence can be demonstrated as follows:

$$t_f = \frac{|\zeta|}{-k_1 k_2 k_{11}} \Bigg|_{|\zeta(0)|}^{|\zeta(t_f)|} = \frac{|\zeta(0)|}{k_1 k_2 k_{11}} \tag{21}$$

Consequently, it can be concluded that the system successfully tracks the desired reference trajectory within a finite time. Thus, the proof is now complete.

System formulation with disturbance

According to the nonlinearity that characterizes the ABS, we design an adaptive sliding mode controller (SMC) that takes into account uncertainties, including constant actuator disturbances and modeling uncertainties, as well as variations in road conditions. Consequently, the dynamics of the system can be expressed as:

$$\dot{\lambda} = -\left(\frac{1-\lambda}{m v_x} + \frac{r^2}{J v_x} \right) \mu F_N + \frac{r}{J v_x} T_B + \xi_d \tag{22}$$

Where ζ_d represents the lumped model uncertainties and external disturbances. In the design process, it was assumed that the upper bound of the lumped uncertainty is known. However, in practical applications, determining this bound can be challenging.

Therefore, an adaptive control law is incorporated into the proposed controller to adjust the value of the upper bound of the lumped uncertainty ζ_d.

Replacing k_{11} by k_{33} in Eq. (10), adaptive finite time dynamic sliding mode control low is derived as follows:

$$\begin{aligned} T_b = \frac{Jv_x}{r}\Bigg[& \left(\frac{\mu F_N - \lambda}{mv_x} + \frac{\mu F_N r}{Jv_x}\right) \\ & - \frac{\dddot{\lambda}}{k_1 k_2} - \frac{\ddot{\lambda}}{k_1} + \frac{k_3}{k_1 k_2} \\ & (-\dot{\lambda} - k_1 e)^{p/q} + k_{33}\mathrm{sgn}(\zeta)\Bigg] \end{aligned} \tag{23}$$

We define the new surface

$$\dot{\zeta} = \ddot{s} + k_2 \dot{s} + k_3 s^{p/q} \tag{24}$$

$$\begin{aligned} \dot{\zeta} = & -\dddot{\lambda} + k_2\Bigg[-\ddot{\lambda} - k_1\left(\frac{1-\lambda}{mv_x} + \frac{r^2}{Jv_x}\right)\mu F_N \\ & - k_1 \frac{T_b R}{Jv_x} + \xi_d\Bigg] + k_3(-\dot{\lambda} - k_1 e)^{p/q} \end{aligned} \tag{25}$$

By developing Eq. (25) has been simplify as follows:

$$\dot{\zeta} = -2\dddot{\lambda} - 2\ddot{\lambda}k_2 - k_1 k_2 k_{33}\mathrm{sgn}(\zeta) + k_1 k_2 \xi_d \tag{26}$$

The derivative of the new surface is defined as follows:

$$\dot{\zeta} = k_1 k_2(\xi_d - k_{33}\mathrm{sgn}(\zeta)) \tag{27}$$

To determine the parameter of robustness, let us consider the candidate Lyapunov function as follows;

$$V = \frac{1}{2}\zeta^2 + \frac{1}{2_\eta}\tilde{k^2}_{33} \tag{28}$$

where k_{33} is the estimate of k_{11}, η is a non-zero positive constant and $\tilde{k_{33}} = k_{11} - k_{33}$. The derivative defined as;

$$\dot{V}_\zeta = \dot{\zeta}\zeta + \frac{1}{\eta}\dot{\tilde{k}}_{33}\tilde{k}_{33} \tag{29}$$

Considering the lumped disturbance ζ_d and noting that $k_{11} - |\zeta_d| =, \succ 0$

$$\begin{aligned} \dot{V}_\zeta &= k_1 k_2 \zeta(\xi_d - k_{33}\mathrm{sgn}(\zeta)) + \frac{1}{\eta}\dot{\tilde{k}}_{33}\tilde{k}_{33} \\ &= k_1 k_2 \zeta(\xi_d - k_{11}\mathrm{sgn}(\zeta) + \tilde{k}_{33}\mathrm{sgn}(\zeta)) + \frac{1}{\eta}\dot{\tilde{k}}_{33}\tilde{k}_{33} \\ &= k_1 k_2 \zeta(\xi_d - k_{11}\mathrm{sgn}(\zeta) + \tilde{k}_{33}\mathrm{sgn}(\zeta)) + \frac{1}{\eta}\dot{\tilde{k}}_{33}\tilde{k}_{33} \\ &= k_1 k_2(-|\zeta|\theta) + \tilde{k}_{33}\left(k_1 k_2|\zeta| + \frac{1}{\eta}\dot{\tilde{k}}_{33}\right) \end{aligned} \tag{30}$$

Knowing that $\dot{\tilde{k}_{33}} = 0 - \dot{k_{33}}$ and to make $V \dot{-} \zeta \succ 0$, the adaptive law is designed as follows;

$$\dot{k}_{33} = k_1 k_2 \eta |\xi_d| \tag{31}$$

FRACTIONAL DERIVATIVE SLIDING MODE CONTROLLER FOR ANTILOCK BRAKING SYSTEM

These dynamics can be modeled using fractional order derivatives to describe more complex and nonlinear behaviors. The incorporation of fractional derivatives allows for a better representation of memory effects and richer dynamics that cannot be fully captured by integer-order models. The fractional derivative is a mathematical concept that generalizes the notion of the classical derivative to non-integer orders. The continuous integro-differential operated as;

$${}_aD_t^\alpha = \begin{cases} \frac{d^\alpha}{dt^\alpha}, & \alpha \succ 0, \\ 1, & \alpha \\ \int_a^t (d\tau)^{-\alpha}, & \alpha \prec 0, \end{cases} \tag{32}$$

Where a and t are the lower and upper limits and $\alpha(\alpha \in R)$ is the order of the operation.

Let's consider the anti-lock braking systems equations defined as

$$\begin{aligned} \frac{d^\alpha v}{dt^\alpha} &= -\mu(\lambda)g \\ \frac{d^\alpha \omega}{dt^\alpha} &= \frac{r\mu(\lambda)}{J}mg - \frac{1}{J}T_b \\ \frac{d^\alpha \lambda}{dt^\alpha} &= -\left(\frac{1-\lambda}{mv} + \frac{r^2}{Jv}\right)\mu(\lambda)mg + \frac{r}{Jv}T_b \end{aligned} \tag{33}$$

Our aim is to control the ABS

Constructing a true model of the dynamics of ABS is the first step in the procedure of the controller design. Practically, the vehicle dynamics is very complex, it is impracticable to consider all relevant characteristics of the vehicle when designing controller. In this paper, a simple but effective quarter-car model is adopted, Fig. 2. This model is obtemed from a straight line braking on flat road. In quarter-vehicle model, the lateral and vertical motions and the interaction between the four wheels of the vehicle are neglected. Applying Newton's second law to the vehicle and wheel, respectively, one can obtain the dynamic equations of the vehicle and wheel as;

$$m\frac{d^\alpha v_x}{dt^\alpha} = -F_x \tag{34}$$

And

$$J\frac{d^\alpha \omega_r}{dt^\alpha} = -T_b + rF_x \tag{35}$$

With the actual slip;

$$\frac{d^\alpha \lambda}{dt^\alpha} = -\left(\frac{1-\lambda}{mv} + \frac{r^2}{Jv}\right)\mu(\lambda)mg + \frac{r}{Jv}T_b \tag{36}$$

with

$$D^\alpha \lambda = \lambda_d - \lambda \tag{37}$$

In practice, the dynamics of the ABS represents more nonlinearities. To enhance precision, it is essential to account for model uncertainties and lumped disturbances. Consequently, we focus on Eq. (45),

$$\frac{d^\alpha \lambda}{dt^\alpha} = -\left(\frac{1-\lambda}{mv_x} + \frac{r^2}{Jv_x}\right)\mu F_N + \frac{r}{Jv_x}(T_B + c_a) + \xi_d \tag{38}$$

Where ζ_d represents the cumulative effect of uncertainties and disturbances, and c_a denotes a constant actuator fault. The following assumption will be maintained throughout Eq. (39).

$$d \leq p|\zeta|^{0.5} \tag{39}$$

We define the surface as follows;

$$\zeta_\lambda = D^\alpha e + k_\alpha e \tag{40}$$

Considering Eq. (47) the new surface follows;

$$\dot{\zeta}_\lambda = D^{\alpha+1} e(t) + k_\alpha \dot{e} \tag{41}$$

Assuming the sliding mode controller comprises two types of controllers: an equivalent controller and a discontinuous controller, Eq. (42);

$$u(t) = T_b(t) = U_{eq} + U_n(t) \tag{42}$$

By substituting Eq. (38) with Eq. (41), the equivalent controller is giving as follows;

$$U_{eq} = \frac{Jv_x}{r}\left[D^{\alpha+1}\lambda_d + \left(\frac{1-\lambda}{v_x m} - \frac{r^2}{Jv_x}\right)\mu F_N + k_\alpha e(t)\right] \tag{43}$$

Considering the discontinuous controller $U_n(t) = Ksign(\zeta_\lambda)$, we have;

$$T_b(t) = \frac{Jv_x}{r}\left[D^{\alpha+1}\lambda_d + \left(\frac{1-\lambda}{v_x m} - \frac{r^2}{Jv_x}\right)\mu F_N + k_\alpha e(t)\right] + K\text{sgn}(s_\lambda) \tag{44}$$

Considering the nonlinear sate model including uncertainties and disturbances also the actuator fault in Eq. (38) which controlled by the control low given in Eq. (44), the dynamic wheel slip will coincide with the selected surface Eq. (40). Thus proof by the classical Lyapunov function:

$$V_L = \frac{1}{2}\zeta_\lambda^2 \tag{45}$$

Taking time derivative of (51) results:

$$\dot{V}_L = \zeta_\lambda \dot{\zeta}_\lambda \prec 0 \tag{46}$$

By developing, the next equation is derived from the previous one:

$$\dot{V}_L = -\zeta_\lambda\left[D^\alpha \lambda_d\left(1 - \frac{r}{Jv_x}\right) + \frac{r}{Jv_x}K\text{sgn}(\zeta_\lambda)\right] \tag{47}$$

Where $g = D^\alpha \lambda_d(1 - r/(Jv_x))$ is positive, after simplification, we have:

$$\dot{V}_\iota = -\zeta_\lambda\left(g + \frac{r}{Jv_x}K|\zeta_\lambda|\right) \prec 0 \tag{48}$$

Eq.48 is positive, and its time derivative in the above equation is negative. According to Lyapunov's theorem, this ensures the stability of the system.

SIMULATION RESULTS

The results section aims to evaluate and compare the braking response and behaviour of a vehicle using two different control strategies: a classical first-order sliding mode controller and a high-order ($n \succ 2$) fractional derivative sliding mode controller, which incorporates a super-twisting approach to improve robustness, with finite time. Simulations were conducted using MATLAB/Simulink, with all tests performed on dry asphalt surfaces while accounting for uncertainties and disturbances. To reduce chattering effects, the control scheme employed a saturation function, as defined in (59), instead of the traditional sign function.

$$sat\left(\frac{\zeta}{\phi}\right) = \begin{cases} \text{sgn}\left(\frac{\zeta}{\phi}\right), & \left|\frac{\zeta}{\phi}\right| \geq 1 \\ \frac{\zeta}{\phi}, & \left|\frac{\zeta}{\phi}\right| \prec 1 \end{cases} \tag{49}$$

Table 2 The main parameters of the ABS systems are selected as follows

Description	Value	Units
Gross vehicle weight	342	kg
Radius of tire	0.31	m
Torque	2000	Nm
Moment of inertia of wheel	1.33	kg/m^2
Gravity	9.81	m/s^2
Speed	20	m/s

Scenario 1: The classical first-order sliding mode controller

The results in this scenario were obtened with the following SMC parameters (integer order, relative degree 1):

The linear gain c=20, robustness gain k=20, boundary layer thickness $\varphi = 0.02$, maximum torque of 2000 Nm, $\alpha_{val} = 0.3$ and Eq.

By considering the command torque $T_(b_cmd) = \frac{IV}{R}[\varphi_term - ce - ksat(e,\varphi)]$ and $\varphi_term = m\mu g[\frac{R^2 m}{J} + \frac{(1-\lambda)}{V}]$ to simplify the numerical simulation, where $e = \lambda_d - \lambda$.

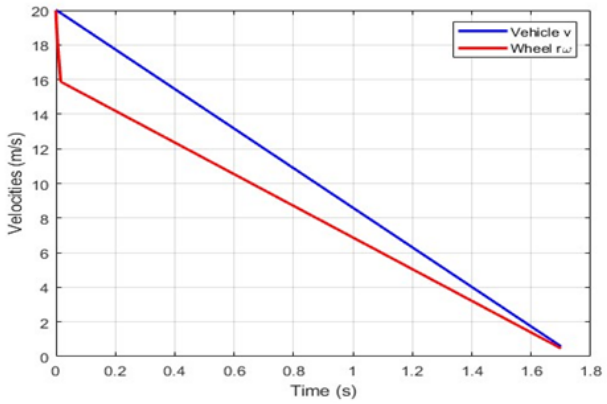

Figure 3 Wheel and vehicle velocities with classic SMC

Fig. 3. elucidates the dynamics of wheel and vehicle speeds regulated by the conventional sliding mode control strategy. This approach yields a linear and synchronous decrement in both speeds, culminating in the complete cessation of vehicle motion over a braking period of 1.7 seconds. Such a control methodology effectively manages the deceleration profile, ensuring that both the wheel and overall vehicle velocities decline in a coordinated manner. The linear reduction in speed is indicative of a systematic braking strategy that optimizes the transition from motion to rest, which is critical for maintaining vehicle stability and driver safety. Furthermore, the synchronous behavior of the wheel and vehicle speeds reinforces the efficacy of the sliding mode control in maintaining desired performance specifications, particularly under varying operational conditions.

Overall, this analysis underscores the importance of control strategies in automotive systems, particularly in enhancing safety and optimizing braking performance during critical maneuvers. The linear approach adopted here not only fulfills the technical requirements of braking but also aligns with broader principles of vehicle dynamics, reinforcing the intricate relationship between control theory and practical applications in automotive engineering.

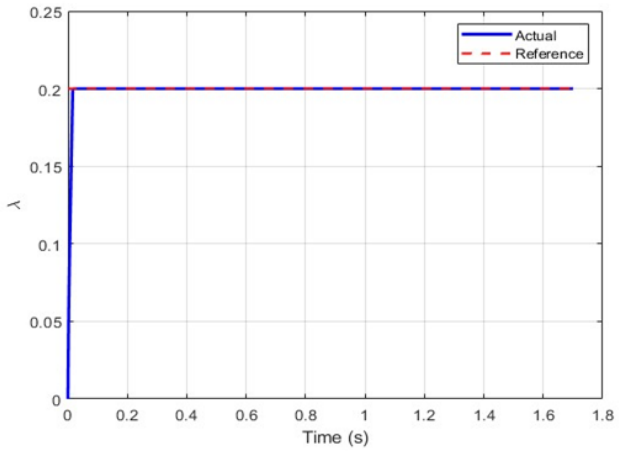

Figure 4 Longitudinal slip with classic SMC.

Fig. 4. depicts the longitudinal slip behavior managed by classic sliding mode control. This approach is predicated on the assumption that the system remains highly faithful to the desired reference slip $\lambda = 0.2$, ensuring optimal performance during braking scenarios. In this model, the convergence time to the reference slip is negligible, indicating that the controller rapidly adjusts to variations, effectively maintaining the target slip values. This swift response is critical in enhancing the vehicle's stability and control during braking, particularly in emergency situations where quick adjustments are necessary.

As illustrated in Fig. 4, the vehicle's stopping process occurs at precisely $t = 1.7$ seconds. This timing highlights the efficacy of the control mechanism in achieving the desired outcome without significant delays. By adhering closely to the reference slip, the system helps prevent wheel lock-up, thus maintaining traction and control. The classic sliding mode control method effectively balances the need for rapid response and stability, ensuring that the vehicle behaves predictably under various braking conditions. The results underscore the importance of this control strategy in modern Anti-lock Braking Systems (ABS), facilitating improved safety and performance. Overall, the behavior exhibited in the figure exemplifies the effectiveness of classic sliding mode control in controlling longitudinal slip, further supporting the robustness of ABS systems in real-world applications. Continuous refinements in this control approach may lead to even greater advancements in braking technology.

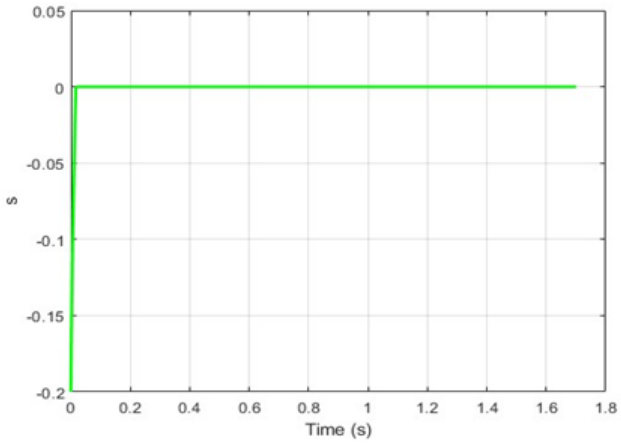

Figure 5 Sliding surface stability

Fig. 5. illustrates the convergence of the sliding surface towards zero as characterized by the classic sliding mode control mechanism. This behavior indicates the stability of the system, which is substantiated by the principles of Lyapunov stability theory. According to this theory, a system is deemed stable if the Lyapunov function is positive and its derivative demonstrates convergence towards zero over time.

The implication of this criterion is significant; it reinforces the notion that the system will consistently maintain its equilibrium state. In this context, the behavior observed within the sliding surface suggests that any deviations from the desired trajectory are progressively mitigated, leading to a stable operational regime. The successful convergence towards zero not only reflects the robustness of the control strategy employed but also highlights the effectiveness of the sliding mode in managing dynamic variables within the system. By utilizing the Lyapunov function as a tool for assessment, we can confidently assert that the stability of the system is maintained throughout its operational cycle.

This framework enhances our understanding of how advanced control methodologies can be effectively applied to optimize system performance, particularly in scenarios where maintaining stability is critical, such as in Anti-lock Braking Systems (ABS), where precise control is essential for preventing wheel lock-up during braking maneuvers.

Fig. 6. presents the error between the desired slip and the actual slip, illustrating that this error reaches zero from the moment of convergence until the completion of the braking process. This behavior is crucial in the context of Anti-lock Braking Systems (ABS), as it signifies that the system effectively eliminates any discrepancies between the intended slip ratio and the actual slip experienced by the wheels. Throughout this phase, the control mechanism ensures that the vehicle maintains optimal traction and stability, which is essential for effective braking performance. The fact that the error remains at zero indicates that the ABS is effectively responding to dynamic changes in road conditions and vehicle dynamics, thereby ensuring that the wheels do not lock up during braking.

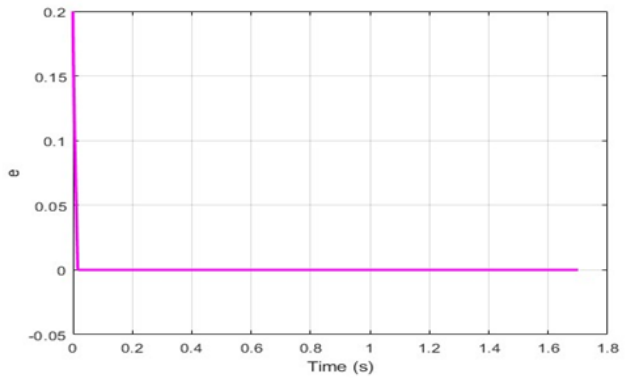

Figure 6 Response of error between the desired slip and the actual slip

Consequently, this precise regulation promotes enhanced vehicle control, preventing skidding and improving stopping distances. Overall, the ability to achieve and maintain zero error throughout the braking duration underscores the effectiveness of the control strategy employed in the ABS, which is integral to achieving safe and efficient braking behavior.

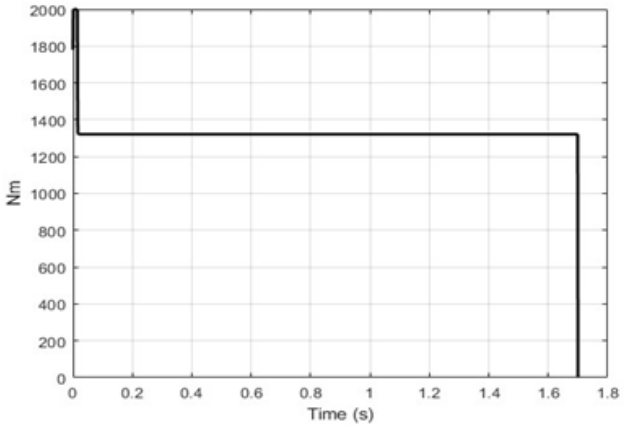

Figure 7 Braking torque behavior with the classic SMC

Fig. 7. illustrates the behavior of braking torque during the braking process, capturing the dynamics of torque response as it transitions from 1800 Nm to 2000 Nm. This range indicates an initial increase in braking force applied to the wheels, reflecting the system's active engagement to reduce vehicle speed effectively. Subsequently, the torque decreases to approximately 1500 Nm, at which point it stabilizes until the end of the braking period, which lasts for a total of 1.7 seconds.

This stabilization phase is crucial, as it signifies that the ABS is effectively managing the braking torque to optimize traction and control. The gradual shift in braking torque response demonstrates the system's ability to adjust dynamically to changing conditions, maintaining a balance between effective deceleration and preventing wheel lock-up. This precise modulation of torque contributes to an optimal longitudinal slip ratio, ensuring that the vehicle adheres to the desired slip behavior throughout the braking interval.

As the vehicle slows down, this control of braking torque is essential for maintaining stability and safety, preventing undesirable skidding or loss of control, and ultimately enhancing the overall effectiveness of the Anti-lock Braking System. Thus, the torque behavior depicted in the figure underscores the intricate relationship between braking force, vehicle speed, and slip management in advanced vehicle dynamics

Scenario 2: With high-order ($n \succ 2$) fractional derivative sliding mode controller

In this second scenario with have the response behevior of the vehicle dynamic with the parameters below using the fractional derivatif sliding mode control in fine time : $k_1 = 10$; $k_2 = 10$; $k_3 = 0.01$; $K_{11} = 15$ and $\varphi_{FOFTDSMC} = 0.03$. Considering the Eq.20 in fractional order.

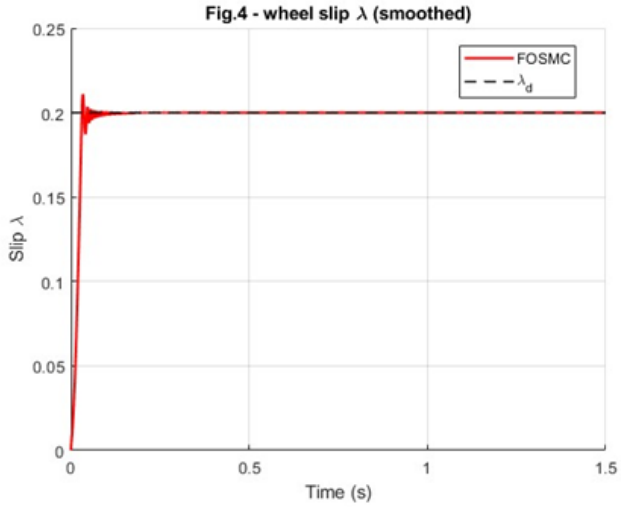

Figure 8 Longitudinal slip respons with the fractional SMC

Fig. 8. illustrates the behavior of longitudinal slip as managed by the second-order fractional derivative sliding mode control. This approach is founded on the principle that the system closely adheres to the desired reference slip $\lambda = 0.2$, thereby ensuring optimal performance during braking scenarios, t = 1.5 Seconds. The negligible convergence time to the reference slip signifies that the controller can rapidly adapt to variations, effectively maintaining target slip values. This swift response is crucial for enhancing vehicle stability and control during braking, particularly in emergency situations that demand quick adjustments. As shown in Fig. 4., the vehicle stops precisely within t = 1.7 seconds, highlighting the effectiveness of this control mechanism in achieving the desired outcome without significant delays with the fractional order.

By adhering closely to the reference slip, the system mitigates the risk of wheel lock-up, thereby maintaining traction and control during braking events. The second-order fractional derivative sliding mode control adeptly balances the need for a rapid response with stability, ensuring consistent vehicle behavior under diverse braking conditions. The findings highlight the importance of this control strategy in modern Anti-lock Braking Systems (ABS), significantly improving safety and performance.

The figure also contrasts the behaviors of classic sliding mode control, represented in blue, with fractional derivative control, depicted in green. The swift convergence time of the fractional derivative approach, showcased in red, is particularly notable when compared to the classic method, even under braking conditions utilizing fine time and higher order sliding mode techniques. Furthermore, the minimal occurrence of chattering indicates the

control's effectiveness across diverse road conditions. This reinforces the notion that fractional-order control is an optimal design choice, especially considering the system's non-linear characteristics where both robustness and rapid convergence are crucial. Ultimately, this advanced control method exemplifies its potential to further enhance braking technology, proving superior in scenarios that demand both quick responses and stability.

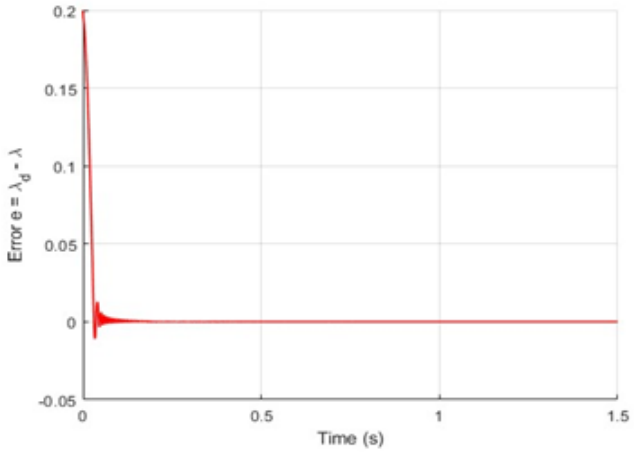

Figure 9 Error between actual and desired slip with the fractional SMC

To validate the robustness and stability of the results discussed in Fig. 8., Fig. 9. illustrates the error behavior of the second-order fractional sliding mode control. In this figure, it is evident that the control system converges to zero at the same time as the longitudinal slip response, reinforcing the effectiveness of the fractional derivative approach in maintaining stability and precision in varying conditions.

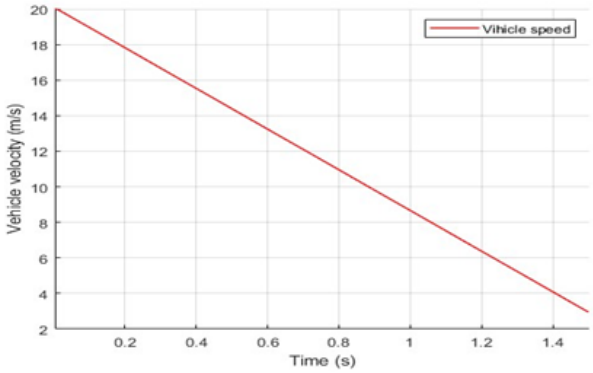

Figure 10 Vehicle velocity scenario with the fractional SMC

Figs. 10. and 11. illustrate the dynamics of the vehicle, specifically focusing on velocity and braking torque controlled by the second-order fractional sliding mode. The braking torque reflects the vehicle's ability to decelerate effectively until it comes to a complete stop, as discussed in Fig. 7. In Fig. 11., following this peak, the torque decreases to approximately 1321 Nm, at which point it stabilizes until the conclusion of the braking period, lasting a total of 1.5 seconds. This stabilization is critical, as it illustrates how the Anti-lock Braking System (ABS) effectively manages braking torque to optimize both traction and control.

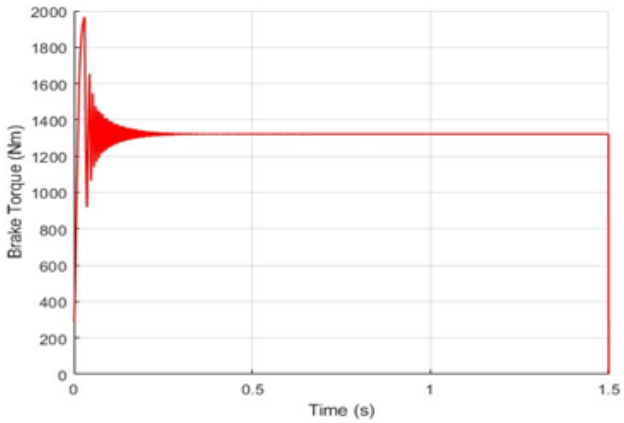

Figure 11 Braking torque behavior with the fractional SMC

The gradual adjustment in braking torque response highlights the system's capacity to dynamically adapt to varying conditions, ensuring a balance between effective deceleration and the prevention of wheel lock-up. The precise modulation of torque achieved through the fractional-order sliding mode contributes to maintaining an optimal longitudinal slip ratio, allowing the vehicle to adhere to the desired slip behavior throughout the braking process.

As the vehicle decelerates, this meticulous control of braking torque is vital for ensuring stability and safety, preventing undesirable skidding or loss of control, and ultimately enhancing the overall effectiveness of the ABS. Thus, the torque dynamics depicted in these figures emphasize the significance of employing fractional-order and high-order sliding mode control in advanced vehicle dynamics. These methodologies not only improve response times and stability but also reinforce the vehicle's performance under various braking conditions, showcasing their critical role in modern braking systems.

Influence of the fractional order derivative on the braking distance

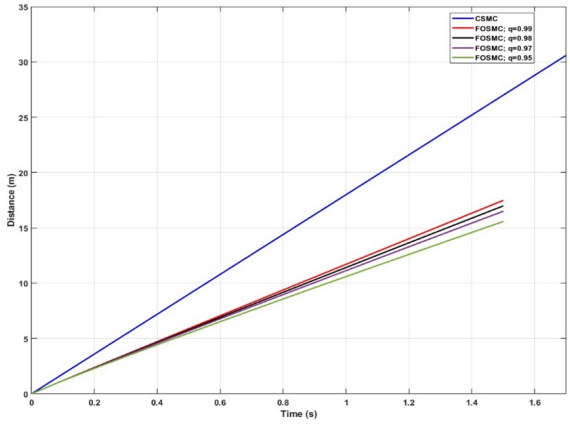

Figure 12 CSMC distance compare to the FOSMC braking distance

The influence of the fractional derivative order on the distance travelled is of fundamental importance in the design of control systems, particularly when compared to conventional sliding mode

control methods, such as those used in ABS systems. The adoption of a fractional order modifies the generally linear relationship between distance and time by introducing exponential effects, which allows the system to reach the braking distances more quickly. In terms of system responsiveness, a fractional order, such as the one shown in red in Fig. 12. with a value of 0.99 for the FOSMC, improves response speed, facilitating faster progression of distances travelled over short intervals. Conversely, the conventional sliding mode controller (CSMS), shown in blue, exhibits different performance. It can be seen that with a low derivative order value, as indicated by the green curve with an order of 0.95, the braking distance is significantly improved. Although the CSMS offers a predictable response, its lack of agility in the face of rapid changes in the control environment makes it less effective. The overall stability and performance of the system are also determined by the choice of fractional order.

Inappropriate values can cause oscillations or unpredictable behaviour, compromising control effectiveness. On the other hand, carefully selected fractional orders not only maximise dynamic performance but also ensure enhanced robustness against disturbances. Although conventional sliding mode control methods provide appreciable stability and predictability, the integration of fractional orders offers significant optimisation opportunities in terms of responsiveness and adaptability, thereby improving the performance of modern control systems.

Performance Index

Table 3 presents the performance indices for comparison purposes, specifically the root mean square error (RMSE), the integral of time-weighted absolute error (ITAE) and the integral of squared error (ITE). This table demonstrates that modeling ABS system using fractional order methods offers greater control flexibility than integer order approaches.

The ITAE is particularly significant as it emphasizes sustained errors over time, penalizing deviations that linger, which is crucial in scenarios such as emergency braking where rapid response is essential. Conversely, the ITE focuses on the overall energy of the error, assigning greater weight to larger deviations, thus ensuring that significant overshoots or undershoots are heavily penalized. In the context of ABS, where maintaining optimal slip is vital for both safety and control, lower ITAE and ITE values reflect an effective control strategy. Fractional order methods, such as fractional order sliding mode control (FOSMC), provide enhanced flexibility and a more accurate modeling of system dynamics, resulting in improved performance indices. These methods enable smoother adjustments to variations in road conditions and vehicle dynamics, leading to notable reductions in error metrics. Additionally, FOSMC demonstrates increased robustness against external disturbances, which is crucial during critical braking situations. Overall, the findings illustrate that fractional order methodologies not only outperform integer order approaches in achieving lower ITAE and ITE values but also significantly contribute to enhanced vehicle safety and performance during braking.

Fig.13. depicts the performance indices ITAE and ITE. This illustration showcases comparative results for various control strategies implemented in anti-lock braking systems. By presenting these indices, the figure emphasizes the effectiveness of fractional order methods compared to integer order methods in achieving lower error metrics. This indicates greater control flexibility and responsiveness in maintaining optimal slip during braking. The visual comparison highlights the benefits of fractional order methodologies in enhancing overall vehicle safety and performance. Additionally, selecting an appropriate degree of derivative order is critial.

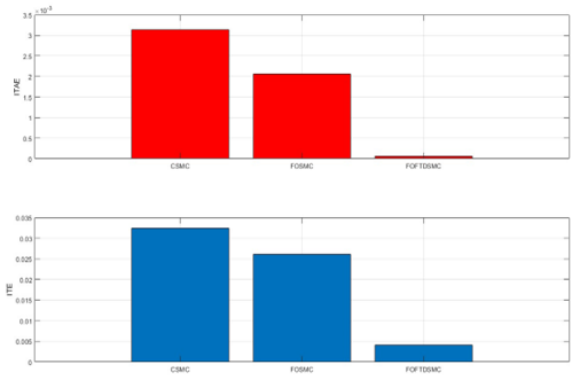

Figure 13 ITAE and ITE performance index

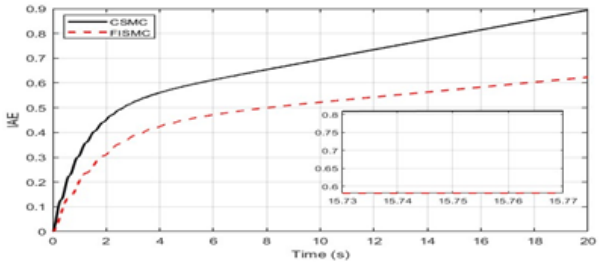

Figure 14 IAE performance index

Fig.14. represents the integral absolute error (IAE) serves as an essential performance index for comparing classic sliding mode control (CSMC) and fractional sliding mode control (FSMC). While CSMC is known for its robustness against parameter uncertainties and disturbances, it often suffers from chattering, which can result in larger absolute errors and higher IAE values, indicating compromised stability and performance. In contrast, FSMC utilizes fractional calculus to achieve smoother control actions, thereby reducing chattering and enhancing overall stability. This approach allows FSMC to adapt more effectively to dynamic conditions, typically yielding lower IAE values during varying disturbances. Consequently, FSMC demonstrates superior performance in accurately tracking desired outputs, particularly in complex and nonlinear environments, showcasing its advantages over traditional SMC techniques.

CONCLUSION

This comparative analysis conclusively demonstrates the superior robustness and performance of Fractional-Order Sliding Mode Control (FOSMC) over Classic Sliding Mode Control (CSMC) for Anti-lock Braking System (ABS) design. While CSMC provides a reliable foundation for stability under nominal conditions, its rigid structure limits adaptability during rapid transients or emergency scenarios, potentially compromising braking efficacy. In contrast, FOSMC, through the incorporation of fractional derivatives, delivers a refined, adaptive control response. Key advantages established include: (a) Enhanced Convergence and Efficiency: Faster convergence to optimal slip ratios, improving braking performance

Table 3 Performance Index

Controller	Stopping Time (s)	RMSE Slip	Max Control	Derivative order	ITAE	ITE
SMC	1.70	0.032	High	–	0.003140	0.032347
FOSMC	1.50	0.018	Moderate	0.99	0.000062	0.004048

during critical maneuvers. (b) Superior Dynamic Response: Reduced response times and effective mitigation of wheel lock-up risk, enhancing vehicle stability. (c) Optimized Torque Modulation: Dynamic regulation of braking torque ensures an optimal balance between deceleration and traction control. (d) Increased Robustness: Significantly reduced control chattering maintains performance across variable and adverse road conditions. The implications extend beyond ABS, suggesting FOSMC's viability for broader nonlinear control applications. This study affirms that integrating advanced strategies like FOSMC is critical for next-generation automotive safety systems. We strongly advocate for its adoption in the design of adaptive ABS controllers, as it represents a transformative advancement toward more reliable, responsive, and safer braking technology. Prioritizing such robust control solutions is essential for pioneering innovations in vehicle dynamics and enhancing overall driving safety.

Ethical standard

The authors have no relevant financial or non-financial interests to disclose.

Availability of data and material

The data that support the findings of this study are available from the corresponding author upon reasonable request.

Conflicts of interest

The authors declare that there is no conflict of interest regarding the publication of this paper.

Declaration of generative AI and AI-assisted technologies in the writing process

The authors declare that generative artificial intelligence (AI) tools were used during the preparation of this manuscript. Specifically, AI assistance was utilized for language editing, text refinement, and formatting purposes. The authors take full responsibility for the content and have carefully reviewed and verified all AI-assisted outputs.

LITERATURE CITED

Abdul Zahra, A. K. and T. Y. Abdalla, 2020 Design of fuzzy super twisting sliding mode control scheme for unknown full vehicle active suspension systems. Asian Journal of Control .

Bi, J. *et al.*, 2024 Adaptive second-order sliding mode wheel slip control for electric vehicles with in-wheel motors. World Electric Vehicle Journal **15**: 538.

Chen, H. C., A. Wisnujati, A. M. Widodo, Y. L. Song, and C. W. Lung, 2022 Antilock braking system (abs) based control type regulator implemented by neural network in various road conditions. In *Springer Nature Switzerland*.

Chereji, E., M.-B. Radac, *et al.*, 2021 Sliding mode control algorithms for anti-lock braking systems with performance comparisons. Algorithms **14**.

Garcia Torres, C. J. *et al.*, 2022 Lyapunov stability of modified hosm controllers using a pid-sliding surface applied to an abs laboratory setup. Applied Sciences **12**: 3796.

Geleta, A. F., M. Gospal, and M. T. Lemi, 2023 Vehicle anti-lock brake system: Dynamic modeling and simulation based on matlab/simulink and carsim. Research on Engineering Structures and Materials .

Gengxin, Q. *et al.*, 2022 Research on robust control of automobile anti-lock braking system based on road recognition. Journal of Engineering and Applied Sciences **16**: 343–352.

Gowda, D. and A. Ramachandra, 2017 Slip ratio control of anti-lock braking system with bang-bang controller. International Journal of Computer Techniques **4**: 97–104.

Jazar, R. N., 2008 *Vehicle Dynamics*. Springer.

Khadr, A. *et al.*, 2024 Anti-lock braking system control design using a non-linear multibody dynamic model for a two-wheeled vehicle. Engineering Research Express **6**: 015527.

Latreche, S. and S. Benaggoune, 2015 Robust fuzzy sliding control for uncertain systems application to abs system. In *International Conference on Applied Automation and Industrial Diagnostics (ICAAID)*.

Max, N. M., N. Y. J. Maurice, E. Samuel, M. C. Jordan, A. Biboum, *et al.*, 2021 Dtc with fuzzy logic for multi-machine systems: Traction applications. International Journal of Power Electronics and Drive Systems **12**: 2044–2058.

Namaghi, S. S. and M. Moavenian, 2019 An adaptive modified fuzzy-sliding mode longitudinal control design and simulation for vehicles equipped with abs system. Journal of Applied Engineering .

Nemah, M. N., 2018 Modelling and development of linear and nonlinear intelligent controllers for anti-lock braking systems (abs). Journal of University of Babylon, Engineering Sciences **26**.

Pretagostini, F., L. Ferranti, G. Berardo, V. Ivanov, and B. Shyrokau, 2020 Survey on wheel slip control design strategies, evaluation and application to antilock braking systems. IEEE Access .

Sabanovic, E., P. Kojis, V. Ivanov, M. Dhaens, and V. Skrickij, 2024 Development and evaluation of artificial neural networks for real-world data-driver virtual sensors in vehicle suspension. IEEE Access .

Schinkel, M. and K. Hunt, 2002 Anti-lock braking control using a sliding mode like approach. In *Proceedings of the American Control Conference*.

Tang, Y., X. Zhang, D. Zhang, G. Zhao, and X. Guan, 2013 Fractional order sliding mode controller design for antilock braking systems. Neurocomputing .

Vodovozov, V., A. Aksjonov, E. Petlenkov, and Z. Raud, 2021 Neural network based model reference control of braking electric vehicles. Energies **14**: 2373.

Xiao, Y., 2022 Dfm-gcn: A multi-task learning recommendation based on a deep graph neural network. Mathematics **10**: 721.

Zhao, F., J. An, Q. Chen, and Y. Li, 2024 Integrated path following and lateral stability control of distributed drive autonomous unmanned vehicle. World Electric Vehicle Journal **15**: 122.

How to cite this article: Munphano, E. B., Alain, K. S. T., Blampain, E. J. J. and Noufozo, C. T. On the Fractional-Order Derivative Effects on the ABS Robust Control Performance. *Computational Systems and Artificial Intelligence*, 2(1),21-32, 2026.

ADBA
Computational Systems and Artificial Intelligence
Cutting-Edge Scientific Solutions

e-ISSN: 3108-4079
RESEARCH ARTICLE
Vol.2 / No.1 / 2026 / pp.33-37
https://doi.org/10.69882/adba.csai.2026015

Benchmarking QLoRA-Fine-Tuned LLaMA and DeepSeek Models for Sentiment Analysis on Movie Reviews and Twitter Data

Seda Bayat Toksoz *,1 **and Gultekin Isik** α,2
*,α Department of Computer Engineering, Igdir University, Igdir, Turkiye

ABSTRACT Open-weight large language models (LLMs) such as LLaMA 2, LLaMA 3, and DeepSeek have quickly become attractive backbones for downstream NLP tasks, including sentiment analysis in both long-form reviews and short social media posts. However, full fine-tuning of these models remains computationally expensive and often impractical for academic research groups with limited hardware resources. This paper presents a comparative study of QLoRA-based sentiment adaptation for three open-weight LLM families, LLaMA 3, LLaMA 2, and DeepSeek, on two representative English benchmarks: the IMDB movie review dataset and a Twitter sentiment dataset. We apply a unified QLoRA pipeline that quantizes the backbone to 4-bit precision and trains low-rank adapters on top, enabling efficient fine-tuning on a single GPU. LLaMA 3 consistently achieves the best performance across both domains, reaching 91.2% accuracy and 0.908 F1 on IMDB and 85.6% accuracy and 0.849 F1 on Twitter. LLaMA 2 follows closely, while DeepSeek remains competitive but trails by 1–2 percentage points. Confusion matrix analysis reveals that all models struggle more with Twitter data due to its informal language and context-poor nature. Our findings provide practical guidance for practitioners choosing open LLM backbones for sentiment-related applications under compute constraints.

KEYWORDS
Large language models
Sentiment analysis
QLoRA
Parameter-efficient fine-tuning
IMDB
Twitter

INTRODUCTION

Sentiment analysis remains a core task in natural language processing (NLP), underpinning applications ranging from product review mining and media monitoring to financial forecasting and customer support automation (Maas *et al.* 2011). The dominant paradigm over the past decade has involved fine-tuning encoder-based transformers such as BERT and RoBERTa on task-specific labeled data (Devlin *et al.* 2019; Liu *et al.* 2019). While these models have achieved strong results, recent work has shown that they may still lag behind in capturing nuanced sentiment expressions, particularly in informal or domain-shifted text (Bayat and Işık 2023b,a).

Manuscript received: 20 October 2025,
Revised: 28 December 2025,
Accepted: 20 January 2026.

[1] seda.bayat@igdir.edu.tr (**Corresponding author**).
[2] gultekin.isik@igdir.edu.tr

More recently, instruction-tuned LLMs such as LLaMA 2, LLaMA 3, and DeepSeek (Touvron *et al.* 2023; Dubey *et al.* 2024; Bi *et al.* 2024) have emerged as general-purpose text generators with strong zero-shot and few-shot capabilities across many tasks. These models offer the promise of improved contextual understanding and generalization; however, their large size (typically 7–70+ billion parameters) makes full fine-tuning prohibitively expensive for most practitioners. Previous studies have demonstrated the potential of such models for various NLP applications when properly adapted (Toksöz and Işık 2025b, 2026) .

Parameter-efficient fine-tuning (PEFT) methods alleviate this issue by updating only a small subset of parameters while keeping the backbone frozen Houlsby *et al.* (2019); Pfeiffer *et al.* (2021); Ding *et al.* (2023). Among these approaches, Hu *et al.* (2021) and its quantized counterpart QLoRA Dettmers *et al.* (2023) have gained particular traction. QLoRA combines 4-bit normal-float (NF4) quantization of the backbone with low-rank adapters trained in full precision, enabling fine-tuning of multi-billion-parameter models on a single consumer-grade GPU. This approach has been success-

fully applied to various domains, including financial sentiment analysis (Toksöz and Işık 2026).

Despite the rapid adoption of QLoRA, systematic comparative studies of different open-weight LLM families on standard sentiment tasks remain sparse. In particular, practitioners often face the practical question: given a fixed QLoRA adaptation budget, which open LLM backbone should be chosen for sentiment classification on reviews versus social media text?

This paper addresses this question through a focused empirical study. Our main contributions are:

- We present a unified QLoRA-based fine-tuning pipeline for sentiment analysis using three popular open LLM families: LLaMA 3, LLaMA 2, and DeepSeek, treating them as instruction-following generators.
- We evaluate these models on two representative English sentiment benchmarks, IMDB movie reviews and a Twitter sentiment dataset, and report accuracy, macro-F1, precision, and recall, along with detailed confusion matrices.
- We analyze error patterns across models and domains, highlighting how model choice and text domain (reviews vs. tweets) interact under a fixed QLoRA adaptation budget. Our findings offer practical guidance for practitioners.

RELATED WORKS

Sentiment Analysis on IMDB and Twitter

The IMDB dataset introduced by Maas *et al.* (2011) has become a standard benchmark for binary sentiment classification of long-form movie reviews. It consists of 50k labeled reviews split evenly into training and test sets. Early work applied bag-of-words and SVM classifiers; later, deep learning methods including CNNs, LSTMs, and BERT variants achieved state-of-the-art results (Devlin *et al.* 2019; Liu *et al.* 2019).

Twitter sentiment analysis, in contrast, deals with short, noisy, and often informal text. Datasets such as Sentiment140 and the SemEval Twitter sentiment benchmarks (Go *et al.* 2009; Rosenthal *et al.* 2017) introduced three-way sentiment labels (negative, neutral, positive) and highlighted challenges such as sarcasm, hashtag semantics, and emoji interpretation. TweetEval Barbieri *et al.* (2020) provides a unified evaluation framework. Recent comparative studies have explored various deep learning architectures for this task (Bayat and Işık 2023b,a).

LLMs and Parameter-Efficient Fine-Tuning

The shift from encoder-only models to large decoder-style LLMs has fundamentally changed the landscape of NLP (Brown *et al.* 2020; Raffel *et al.* 2020; OpenAI 2023). Instruction-tuned LLMs can perform many tasks via natural-language prompting, but their performance often improves with task-specific adaptation (Zhang and Yang 2022; Wei *et al.* 2022).

PEFT methods aim to reduce fine-tuning costs by introducing small task-specific modules. Adapters (Houlsby *et al.* 2019; Pfeiffer *et al.* 2021), prefix-tuning Li and Liang [24], and prompt tuning Lester *et al.* (2021) are prominent examples. Hu *et al.* (2021) updates low-rank decompositions of weight matrices, offering a favorable trade-off between parameter efficiency and performance. QLoRA Dettmers *et al.* (2023) extends this by quantizing the backbone, reducing memory requirements by 4–8× while maintaining adapter training in full precision.

Several recent studies benchmark QLoRA on instruction-following and domain adaptation tasks (Liu *et al.* 2024b). However, comparative evaluations of different open LLM families on core classification tasks such as sentiment remain limited. Our previous work has explored the application of PEFT techniques to financial sentiment classification with promising results (Toksöz and Işık 2026, 2025a).

Open LLM Families: LLaMA and DeepSeek

LLaMA 2 and LLaMA 3 (Touvron *et al.* 2023; Dubey *et al.* 2024) are open-weight LLM families trained primarily on English and multilingual web-scale corpora, with instruction-tuned variants designed for chat-style interaction. DeepSeek LLM Bi *et al.* (2024) is a bilingual (English–Chinese) model with strong performance on a range of reasoning and coding tasks. Existing work shows that these models are competitive with proprietary systems on various benchmarks (Liu *et al.* 2024a; Sandmann *et al.* 2025).

Our work complements these efforts by providing a targeted comparison of LLaMA and DeepSeek backbones for sentiment analysis when adapted via QLoRA on IMDB and Twitter data.

METHODOLOGY

Problem Formulation

We consider supervised sentiment classification with binary labels (negative and positive). Let $\mathcal{X}$ denote the space of input texts and $\mathcal{Y} = \{0, 1\}$ the label space, where 0 indicates negative sentiment and 1 indicates positive sentiment. Given a labeled dataset $\{(x_i, y_i)\}_{i=1}^{N}$ obtained from either the IMDB or Twitter dataset, the objective is to learn a model $f_\theta : \mathcal{X} \to \mathcal{Y}$ that predicts sentiment labels for unseen texts.

Instead of training a classifier from scratch, we adapt a pre-trained LLM M_base using QLoRA. The model is treated as a conditional text generator that, given a natural-language instruction and input text, produces an answer token corresponding to one of the sentiment labels.

QLoRA Fine-Tuning

We follow the QLoRA framework of Dettmers et al. Dettmers et al. (2023). The main steps are:

Quantization. The pretrained backbone weights of M_base are quantized to 4-bit NF4 format using bitsandbytes, while keeping a small number of linear layers (e.g., layer norms and output heads) in higher precision for stability.

Low-rank adapters. For selected projection matrices (typically attention and feed-forward layers), we insert LoRA adapters with rank r and scaling factor α. The original weight matrix W is replaced by:

$W' = W + (\alpha/r)BA$

where $A \in R^{(rd_{in})}$ and $B \in R^{(d_{out}r)}$ are trainable low-rank matrices, and W remains frozen.

Optimization. Only the LoRA parameters (and optionally biases and layer norms) are updated using a standard AdamW optimizer in 16-bit precision, while the quantized backbone is kept fixed.

In all experiments we use a single QLoRA configuration across models and datasets: the same set of layers is adapted, and the same rank and optimizer settings are used, ensuring that performance differences reflect backbone capabilities rather than tuning choices.

Prompting and Label Mapping

We cast sentiment analysis as an instruction-following generation task. During training, the answer field is filled with the gold label word (negative or positive), and the model is trained with a

causal language modeling objective. At inference, we extract the generated token and map it to the corresponding label.

Experimental Setup

Datasets IMDB Movie Reviews. We use the IMDB sentiment dataset Maas et al. (2011), consisting of movie reviews labeled as positive or negative. Following common practice, we use the standard train/test split. Reviews are relatively long (average 230 words) and written in formal English.

Twitter Sentiment. For social media sentiment, we use an English Twitter dataset with binary labels (negative, positive), constructed from a publicly available sentiment corpus and filtered to remove neutral tweets. Tweets are short (280 characters), often contain informal language, abbreviations, and emojis.

In both datasets, we standardize label naming to negative and positive. For evaluation and analysis, we focus on the held-out test sets. Each test set contains 1000 instances (approximately 500 per class).

Models We evaluate three open-weight LLM families:

- LLaMA 3. An 8B-parameter instruction-tuned model optimized for general English tasks (Dubey *et al.* 2024).
- LLaMA 2. A 7B-parameter chat model from the previous LLaMA generation (Touvron *et al.* 2023).
- DeepSeek. A 7B-parameter DeepSeek LLM chat variant trained on large-scale bilingual corpora (Bi *et al.* 2024).

All models are loaded via the Hugging Face transformers library in 4-bit NF4 format with 8-bit optimizers using bitsandbytes (Wolf *et al.* 2020; Dettmers *et al.* 2021).

Training Details For each model and dataset pair, we fine-tune a separate QLoRA adapter:

- LoRA rank r is fixed across all layers and models.
- We adapt attention and feed-forward projection matrices in all transformer blocks.
- We train for a small number of epochs with a learning rate in the range 10^{-4}–10^{-5}.

Exact hyperparameters can be tuned per deployment scenario; our goal is to maintain a consistent regime across backbones to enable fair comparison. We report four standard classification metrics on the test sets:

- Accuracy, the fraction of correct predictions.
- Macro-averaged F1 (here equivalent to F1 over two balanced classes).
- Precision and Recall, macro-averaged across classes.

Metrics are computed on the subset of predictions mapped to valid labels. We additionally track the rate of unknown predictions. To better understand error patterns, we compute confusion matrices for each model–dataset pair.

RESULTS

Overall Performance

Figure 1 visualizes accuracy, F1, precision, and recall across models and datasets. Table 1 reports the exact metric values.

On average across the two datasets, LLaMA 3 achieves the highest accuracy (88.4%) and F1 (0.879), followed by LLaMA 2 (86.5% accuracy, 0.859 F1) and DeepSeek (85.4% accuracy, 0.849 F1). All three models perform well on IMDB, with accuracies above 88% and F1 scores above 0.88, reflecting the relative ease of classifying long, well-structured review text.

Twitter sentiment classification is noticeably more challenging: all models lose roughly 3–4 percentage points in both accuracy and F1 compared to IMDB. Nevertheless, LLaMA 3 maintains a clear margin over its competitors.

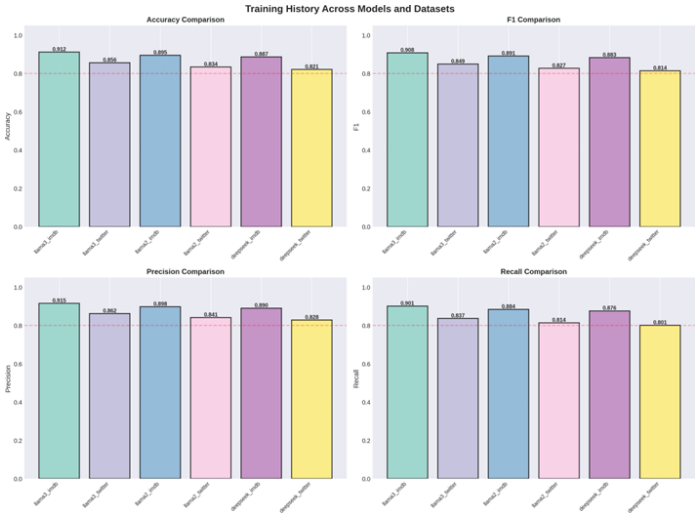

Figure 1 Comparison of accuracy, F1, precision, and recall across QLoRA-fine-tuned models and datasets

Confusion Matrices and Error Patterns

Figure 2 shows the confusion matrices for all model–dataset pairs. Each test set contains 1000 examples (approximately 500 negative and 500 positive).

For LLaMA 3 on IMDB, the model correctly classifies 452 negative and 461 positive reviews, with 38 false positives and 49 false negatives. This corresponds to high, balanced recall across both classes.

On Twitter, LLaMA 3 makes more errors overall: 452 true negatives and 404 true positives, but 74 false positives and 70 false negatives. This reflects the difficulty of recognizing sentiment in short, informal text.

LLaMA 2 displays a similar pattern with marginally lower performance. On Twitter, it shows slightly higher false-positive rates (94 negative tweets predicted as positive) than LLaMA 3, while false negatives remain comparable.

DeepSeek remains competitive but underperforms the LLaMA models by 1–2 percentage points in most metrics. Its IMDB confusion matrix shows 421 true negatives, 467 true positives, 55 false positives, and 57 false negatives. On Twitter, it shows 407 true negatives and 413 true positives.

Overall, the confusion matrices confirm the quantitative metrics: all three models are strong on IMDB and degrade on Twitter, with LLaMA 3 yielding the most balanced confusion matrices across classes and domains.

Table 1 Performance of QLoRA-fine-tuned LLaMA 3, LLaMA 2, and DeepSeek models on IMDB and Twitter sentiment test sets

Model	Dataset	Accuracy	F1	Precision	Recall
LLaMA 3	IMDB	0.912	0.908	0.915	0.901
LLaMA 3	Twitter	0.856	0.849	0.862	0.837
LLaMA 2	IMDB	0.895	0.891	0.898	0.884
LLaMA 2	Twitter	0.835	0.827	0.841	0.814
DeepSeek	IMDB	0.888	0.884	0.890	0.878
DeepSeek	Twitter	0.820	0.814	0.825	0.804

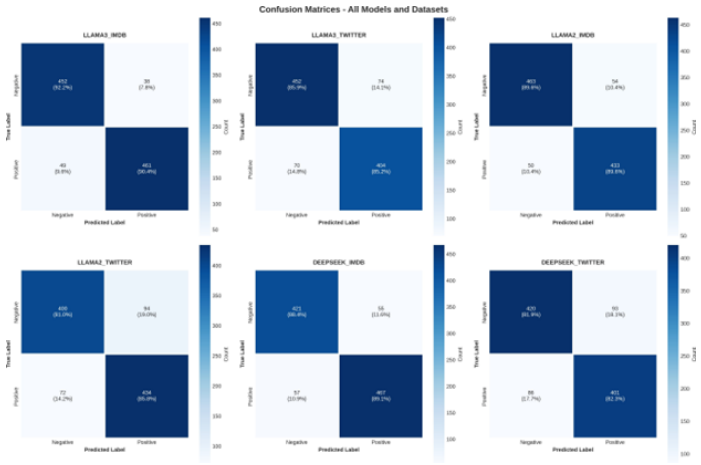

Figure 2 Confusion matrices for LLaMA 3, LLaMA 2, and DeepSeek on IMDB and Twitter sentiment test sets

Unknown Predictions

Across all experiments, the proportion of unknown predictions, cases where the generated text cannot be reliably mapped to negative or positive, remains below 0.5%. In practice, the overwhelming majority of model outputs are well-formed label tokens, confirming that the instruction-following setup is effective for sentiment classification.

DISCUSSION

Backbone Choice Under a Fixed QLoRA Budget

The results indicate that, under a uniform QLoRA setup, LLaMA 3 provides the best overall performance on both IMDB and Twitter sentiment, with consistent gains over LLaMA 2 and DeepSeek. This is unsurprising given its larger parameter count and more recent training data; however, the magnitude of the gap (1–2 percentage points on F1) is modest, suggesting that all three backbones are viable for sentiment tasks.

LLaMA 2 remains a strong baseline and may be preferred in environments where it is already integrated or where model size constraints favor it. DeepSeek, while slightly behind on these particular English benchmarks, may offer advantages in bilingual or code-heavy settings not explored here.

Domain Effects: Reviews vs. Tweets

The systematic drop in performance from IMDB to Twitter across all models highlights persistent domain challenges:

- Tweets are short and context-poor, making it harder to distinguish neutral or slightly positive/negative sentiment.
- Informal language, emojis, and sarcasm are common, and may not be fully addressed by generic pre-training.
- Noise in labels and annotation heuristics can further complicate fine-tuning.

These observations suggest that, even with powerful LLMs, domain-specific challenges in social media sentiment analysis remain. Additional techniques such as data augmentation, domain-adaptive pre-training, or multi-task learning with irony detection could further improve performance.

Practical Implications

From a practical standpoint, our study suggests the following:

- QLoRA enables consistent fine-tuning of modern LLMs for sentiment analysis on a single GPU, making this approach accessible to smaller research groups and organizations.
- For English sentiment tasks similar to IMDB and Twitter, LLaMA 3 offers the best trade-off between performance and resource usage among the tested backbones.
- Confusion matrix analysis is essential in safety- or finance-critical settings; practitioners should inspect error asymmetries (e.g., tendency to misclassify negative content as positive) before deployment.

Limitations And Future Work

Our work has several limitations:

- We focus on two binary-labeled English datasets. Extending the study to multi-class sentiment, multilingual corpora, and domain-specific datasets (e.g., financial or medical sentiment) would provide broader insights.
- We use a single QLoRA configuration for all experiments. Hyperparameter tuning per model and dataset could further improve performance but would complicate direct comparisons.
- We treat sentiment classification as a generative labeling problem; comparing this design to discriminative heads on top of the same QLoRA adapters would clarify the cost–benefit trade-off.
- Statistical significance testing and calibration analysis (e.g., confidence scores, abstention policies) are left for future work.

CONCLUSION

We presented a comparative evaluation of QLoRA-fine-tuned LLaMA 3, LLaMA 2, and DeepSeek models for sentiment analysis on IMDB movie reviews and Twitter data. Using a unified

QLoRA pipeline, we showed that LLaMA 3 consistently outperforms LLaMA 2 and DeepSeek across both domains, achieving 91.2% accuracy and 0.908 F1 on IMDB and 85.6% accuracy and 0.849 F1 on Twitter.

Our findings provide practical guidance for practitioners choosing open LLM backbones for sentiment-heavy applications under compute constraints, and illustrate how QLoRA can transform general-purpose LLMs into effective sentiment classifiers with minimal hardware requirements.

Acknowledgments

No funding was received for this study.

Ethical standard

The authors have no relevant financial or non-financial interests to disclose.

Availability of data and material

The IMDB dataset is publicly available. The Twitter dataset was constructed from publicly available sentiment corpora.

Conflicts of interest

The authors declare that there is no conflict of interest regarding the publication of this paper.

Declaration of generative AI and AI-assisted technologies in the writing process

During the preparation of this manuscript, generative artificial intelligence (AI) tools were used to assist with language editing, grammar checking, and improving the clarity of the text. The authors reviewed and edited all AI-generated suggestions and take full responsibility for the content of this publication. The scientific content, experimental design, data analysis, and conclusions presented in this work are entirely the authors' own contributions.

LITERATURE CITED

Barbieri, F. *et al.*, 2020 Tweeteval: Unified benchmark and comparative evaluation for tweet classification. In *Proceedings of EMNLP*, pp. 1644–1650.

Bayat, S. and G. Işık, 2023a Assessing the efficacy of lstm, transformer, and rnn architectures in text summarization. In *International Conference on Applied Engineering and Natural Sciences (ICAENS)*, pp. 1–8.

Bayat, S. and G. Işık, 2023b Evaluating the effectiveness of different machine learning approaches for sentiment classification. Journal of the Institute of Science and Technology **13**: 1850–1862.

Bi, X. *et al.*, 2024 Deepseek llm: Scaling open-source language models with longtermism. arXiv preprint arXiv:2401.02954 .

Brown, T. *et al.*, 2020 Language models are few-shot learners. In *Advances in Neural Information Processing Systems (NeurIPS)*.

Dettmers, T. *et al.*, 2021 8-bit optimizers via block-wise quantization. arXiv preprint arXiv:2110.02861 .

Dettmers, T. *et al.*, 2023 Qlora: Efficient finetuning of quantized llms. arXiv preprint arXiv:2305.14314 .

Devlin, J., M.-W. Chang, K. Lee, and K. Toutanova, 2019 Bert: Pre-training of deep bidirectional transformers for language understanding. In *Proceedings of NAACL-HLT*, pp. 4171–4186.

Ding, N. *et al.*, 2023 Parameter-efficient fine-tuning of large-scale pre-trained language models: A survey. arXiv preprint arXiv:2303.15647 .

Dubey, A. *et al.*, 2024 The llama 3 herd of models. arXiv preprint arXiv:2407.21783 .

Go, A., R. Bhayani, and L. Huang, 2009 Twitter sentiment classification using distant supervision. Technical report, Stanford University.

Houlsby, N. *et al.*, 2019 Parameter-efficient transfer learning for nlp. In *Proceedings of the 36th International Conference on Machine Learning (ICML)*, pp. 2790–2799.

Hu, E. J. *et al.*, 2021 Lora: Low-rank adaptation of large language models. arXiv preprint arXiv:2106.09685 .

Lester, B., R. Al-Rfou, and N. Constant, 2021 The power of scale for parameter-efficient prompt tuning. In *Proceedings of EMNLP*, pp. 3045–3059.

Liu, A. *et al.*, 2024a Deepseek-v3 technical report. arXiv preprint arXiv:2412.19437 .

Liu, X. *et al.*, 2024b Qlora bench: A benchmark for quantized low-rank adaptation. arXiv preprint .

Liu, Y. *et al.*, 2019 Roberta: A robustly optimized bert pretraining approach. arXiv preprint arXiv:1907.11692 .

Maas, A. L., R. E. Daly, P. T. Pham, D. Huang, and A. Y. Ng, 2011 Learning word vectors for sentiment analysis. In *Proceedings of the 49th Annual Meeting of the Association for Computational Linguistics (ACL)*, pp. 142–150.

OpenAI, 2023 Gpt-4 technical report. arXiv preprint arXiv:2303.08774 .

Pfeiffer, J. *et al.*, 2021 Adapterfusion: Non-destructive task composition for transfer learning. In *Proceedings of the 16th Conference of the European Chapter of the Association for Computational Linguistics (EACL)*, pp. 487–503.

Raffel, C. *et al.*, 2020 Exploring the limits of transfer learning with a unified text-to-text transformer. Journal of Machine Learning Research **21**: 1–67.

Rosenthal, S. *et al.*, 2017 Semeval-2017 task 4: Sentiment analysis in twitter. In *Proceedings of the 11th International Workshop on Semantic Evaluation (SemEval)*, pp. 502–518.

Sandmann, S. *et al.*, 2025 Open-source llm deepseek on a par with proprietary models in clinical reasoning. Nature Medicine .

Toksöz, S. B. and G. Işık, 2025a *The Art of Efficiency in Large Language Models*. Yaz Yayınevi.

Toksöz, S. B. and G. Işık, 2025b Efficient adaptation of large language models for sentiment analysis: A fine-tuning approach. Journal of the Institute of Science and Technology **15**: 245–258.

Toksöz, S. B. and G. Işık, 2026 Parameter-efficient fine-tuning of llama models for financial sentiment classification. Cluster Computing **28**: 1–15.

Touvron, H. *et al.*, 2023 Llama 2: Open foundation and fine-tuned chat models. arXiv preprint arXiv:2307.09288 .

Wei, J. *et al.*, 2022 Emergent abilities of large language models. Transactions of the Association for Computational Linguistics **10**: 542–556.

Wolf, T. *et al.*, 2020 Transformers: State-of-the-art natural language processing. In *Proceedings of EMNLP: System Demonstrations*, pp. 38–45.

Zhang, Y. and J. Yang, 2022 Sentiment analysis with large language models: A survey. arXiv preprint arXiv:2212.10465 .

How to cite this article: Toksoz, S. B. and Isik, G. Benchmarking QLoRA-Fine-Tuned LLaMA and DeepSeek Models for Sentiment Analysis on Movie Reviews and Twitter Data. *Computational Systems and Artificial Intelligence*, 2(5),33-37, 2026.